Editors

Prof. Dr. Edip BAYRAM
Prof. Dr. Nazan YALÇI ERİK

gece kitaplığı

International Research and Evaluations in the Field of Chemical Engineering

October 2025

Genel Yayın Yönetmeni / Editor in Chief • Eda Altunel

Kapak & İç Tasarım / Cover & Interior Design • Gece Kitaplığı

Birinci Basım / First Edition • © Ekim 2025

ISBN • 978-625-388-794-0

Gece Kitaplığı / Gece Kitaplığı
Türkiye Adres / Turkey Address: Kızılay Mah. Fevzi Çakmak 1. Sokak
Ümit Apt No: 22/A Çankaya/ANKARA
Telefon / Phone: 0312 384 80 40

web: www.gecekitapligi.com
e-mail: gecekitapligi@gmail.com

Baskı & Cilt / Printing & Volume
Sertifika / Certificate No: 42488

INTERNATIONAL RESEARCH AND EVALUATIONS IN THE FIELD OF CHEMICAL ENGINEERING

EDITOR

PROF. DR. EDİP BAYRAM
PROF. DR. NAZAN YALÇI ERİK

gece kitaplığı

CONTENTS

Chapter 1

PROTECTIVE COATING SOLUTIONS FOR INDUSTRIAL PIPELINES: ANALYSIS OF ONSHORE AND MARINE APPLICATIONS[1]

Maryam ALIYEVA[2], Nil ACARALI[3]

1 For correspondence: Prof.Dr. Nil ACARALI; nbaran@yildiz.edu.tr
2 Yildiz Technical University, Department of Chemical Engineering, 34220, Esenler-Istanbul, Türkiye.

0009-0002-4443-6781
3 Yildiz Technical University, Department of Chemical Engineering, 34220, Esenler-Istanbul, Türkiye.

Nil Acaralı: 0000-0003-4618-1540

1. INTRODUCTION

Pipelines had always played an important role in industry and had a significant impact on economic development and political relations. The main purpose of the pipeline was to transport whether over long distances or shorter ones [1, 2]. Internal and external corrosion created a significant risk to this type of transportation. In industrial facilities, piping systems were made from various materials depending on several factors, such as the chemical properties of the fluid being transported, along with the temperature and pressure conditions [3]. The severe conditions that surrounded pipelines, fluid friction, leaks, and damaged equipment all caused corrosion. Oxygen, hydrogen, chlorides, and sulphur compounds were the primary substances that caused corrosion [4]. Choosing the right material for a piping system was crucial it affected how strong and efficient the system was and played a major role in keeping the facility safe and running well over time. That was why it was important to carefully check the material's features and ensure it was suitable before using it in an industrial piping system. At that time, the most used materials in industrial piping systems included carbon steel, stainless steel, alloy steels, copper and its alloys, various plastics, and cast iron [5]. Piping systems were not just important for moving fluids but also constituted a key part of modern engineering infrastructure. When designing these systems, factors such as functional requirements, environmental conditions, and the characteristics of the fluids being transported all played a critical role, especially in selecting the right materials. Pipelines were widely used in various sectors, including infrastructure systems and general industrial facilities [6]. Each of these areas came with its own environmental challenges and operating conditions, which affected how likely corrosion was to occur. That was why choosing the right materials was so important. Marine pipelines were essential for transporting petroleum, natural gas, and other fluids between land-based facilities and offshore platforms, or even across long distances under the sea [7]. These pipelines were constantly exposed to tough conditions like salty water, high water pressure, marine life, and changing temperatures. Because of that, coatings applied to marine pipelines required more than simple corrosion prevention and had to resist physical damage and chemical degradation while being compatible with cathodic protection systems [8]. The reliability and efficiency of a pipeline system depended heavily on factors like how well its insulation worked and whether the coating could hold up during underwater operations. This study focused on how environmental conditions affected the choice and performance of these coatings, particularly in terms of corrosion protection, physical strength, and how well the pipelines worked with systems like cathodic protection. This study aimed to offer compre-

hensive insights into optimizing pipeline protection strategies in complex conditions.

2. INDUSTRIAL PIPE MATERIALS

Carbon Steel Pipes:

Carbon steel was widely used in industrial piping because it offered a strong and cost-effective solution [9]. With a carbon content between about 0.05% and 2.1%, it provided the right balance of durability and affordability for many applications [10]. Carbon steel pipes were commonly used to transport steam, water, oil, and natural gas. However, carbon steel pipes could be vulnerable to corrosion in certain environments, often requiring protective coatings or cathodic protection [11]. Because of its strength and ease of welding, carbon steel remained a key material for onshore pipeline systems.

Stainless Steel Pipes:

Stainless steel pipes exhibited excellent high-temperature tolerance and hygienic properties, making them ideal for use in the food, pharmaceutical, and chemical industries [12]. Although the initial cost of stainless steel was higher than that of carbon steel, its long service life and low maintenance requirements often resulted in a lower total cost of ownership. In marine environments, stainless steel was particularly valuable in locations with elevated corrosion risks [13].

Alloy Steel Pipes:

The addition of alloying elements such as nickel, chromium, and molybdenum led to the formation of alloy steels, making them specifically designed to withstand high temperatures and pressures [14]. Alloy steels were often used in power plants, boiler systems, and other high-temperature industrial processes [15]. These steels offered excellent resistance to heat-related expansion and mechanical stress, however, higher manufacturing and processing costs were associated with them compared to regular carbon steel [16].

Copper and Copper Alloy Pipes:

Because of excellent thermal conductivity, resistance to corrosion, and stability in biological environments, copper and its alloys were commonly used in systems, refrigeration lines, and medical gas supplies [17]. However, due to lower mechanical strength compared to some other materials, special care was required when designing systems that operated under high pressure [18].

Polymer-Based Pipes:

Plastic materials such as PVC, CPVC, PE, PP offered many advantages, resistance to chemicals, lightweight nature, and ease of installation [19]. Because of these properties, these materials were often used for transporting chemicals and in systems operating under low to medium pressure. However, vulnerability to damage from UV light, high temperatures, and mechanical stress limited their effective use in certain environments [20].

Ductile Iron Pipes:

Ductile iron pipes had long been used in infrastructure and remained a popular choice for wastewater and sewage systems due to their resistance to wear and noise reduction capabilities [21]. However, the pipes were heavy and somewhat brittle, requiring careful handling during installation and transport.

Selecting the right materials for industrial pipelines involved more than just considering mechanical strength and corrosion resistance. Economic factors, maintenance needs, supply chain logistics, and specific operating conditions all had to be considered. Choosing suitable materials for both onshore and offshore pipelines was essential to ensure the reliability and longevity of industrial facilities. Due to advances in material science and coating technologies, it became possible to develop tailored, efficient, and durable pipeline solutions.

3. APPLICATION AREAS OF PIPING SYSTEMS, CORROSION RISKS, AND MATERIAL SELECTION

3.1 Infrastructure Systems

Infrastructure systems covered a wide variety of services, including drinking water distribution, sewage networks, natural gas pipelines, and storm water drainage [22]. The pipes in these systems were usually buried underground and were directly affected by factors such as soil type, groundwater levels, and environmental pollutants. Metallic pipes were especially prone to corrosion in wet or acidic soils [23]. That was why materials such as plastic pipes, glass fiber reinforced plastic or ductile iron pipes with protective coatings were commonly chosen for these projects [24]. Additionally, internal linings were often added to protect against minerals in the fluids and to reduce corrosion inside the pipes [25]. For drinking water systems, it was especially important to use materials that were chemically stable.

3.2 Industrial Facilities

Piping systems in industrial facilities such as petrochemical plants, refineries, power plants, and food or pharmaceutical factories were essential for keeping operations running smoothly and safely. The fluids transported often faced extreme temperatures, high pressures, and harsh chemical conditions. Because of these challenges, it was important to choose piping materials that were both strong and resistant to corrosion. Systems that transported acids, bases, solvents, or fluids with high chloride content were especially prone to corrosion [26]. That was why materials such as stainless steels, nickel-based alloys, and carbon steel pipes with internal linings were commonly used in these industries [27, 28]. For additional protection, thermoplastic linings such as PTFE or polypropylene were sometimes applied inside pipes [29]. Moreover, double-walled pipes and corrosion monitoring sensors were often installed to enhance safety and reliability in these high-risk environments.

3.3 Steel Manufacturing Industry

The steel production industry represented one of the most aggressive operating environments for piping systems, characterized by high temperatures and exposure to corrosive gases. In processes such as coke oven gas handling, blast furnace gas distribution, and high-temperature steam, pipes were subjected to both thermal fatigue and chemical corrosion [30]. In these situations, choosing the right material involved considering not only corrosion resistance but also the material's mechanical performance at high temperatures. That was why heat-resistant alloys like Cr-Mo steels and ferritic stainless steels were often the materials of choice [31]. To further protect the system, ceramic coatings or refractory linings were applied inside the pipes to reduce wear and guard against sudden temperature changes, thereby extending the system's lifespan. Since steel plants had limited opportunities for planned maintenance, selecting the right materials was especially important to maintain smooth and safe operations.

3.4 Corrosion Protection Strategies

Selecting the right materials was the first line of defense against corrosion, but additional protective measures were often necessary to extend the lifespan of piping systems. Cathodic protection, commonly used for submerged pipelines, worked by reducing electrochemical corrosion through galvanic anodes or impressed current systems. Additionally, coatings such as epoxy, polyurethane-based paints, and zinc-rich primers were widely applied across industries to provide durable, long-term corrosion protection [32].

4. COMPARATIVE ANALYSIS OF COATING REQUIREMENTS AND PERFORMANCE IN INDUSTRIAL ONSHORE AND OFFSHORE ENVIRONMENTS

Onshore (land-based) and offshore (marine) facilities presented fundamentally different challenges in terms of corrosion risk, mechanical stress, maintenance accessibility, and environmental exposure. These differences necessitated special approaches in coating system design, material selection, application methods, and quality control procedures.

4.1 Environmental Exposure and Corrosion Intensity

Onshore environments, depending on their geographic location and type of industry, were usually exposed to typical atmospheric conditions such as sunlight, UV radiation, occasional chemical spills, and changing humidity levels. While these factors caused wear and tear, the conditions were generally less severe compared to offshore settings. Offshore environments, especially those on open sea platforms and coastal areas, faced much tougher challenges. The combination of salty air, constant high humidity, strong wave impacts, marine growth like algae, and frequent temperature changes accelerated corrosion processes. This result led to issues such as pitting, crevice corrosion, and galvanic corrosion, particularly when different metals came into contact in these moist environments. To help manage these risks, corrosivity were categorized from C1 (very low) up to CX (extreme offshore) [33]. Most onshore industrial sites fell into the C3 to C5 range, indicating moderate to high corrosion risk, while offshore structures were often rated C5-M or even CX, reflecting their harsher conditions [34]. Because of this, offshore pipelines required more durable, multi-layered coating systems designed to withstand these extreme environments and protect the infrastructure for as long as possible.

4.2 Material Durability and Coating System Selection

In offshore systems, thermal spray aluminum (TSA) was often used as a high-performance corrosion barrier, especially for parts exposed to splash zones and underwater areas [35]. When combined with sealers or protective topcoats, TSA provided excellent protection against corrosion caused by saltwater and kept structures safe for maintenance-free periods of over 25 years. Offshore coatings typically used multi-layer systems designed for harsh environments and long durability, while onshore coatings were simpler and applied under more controlled conditions, with shorter expected service life. These differences between onshore and offshore coating requirements were also summarized in Table 1.

Table 1. *Material Durability and Coating System Selection for Onshore and Offshore Applications*

Criteria	Onshore Applications	Offshore Applications
Common Coating Systems	Epoxy primers + polyurethane or alkyd topcoats	Multi-coat systems: zinc-rich epoxy primers, epoxy midcoats, polysiloxane or fluoropolymer topcoats
Durability Requirements	10–15 years (moderate conditions)	15–25+ years (high corrosion environment)
Resistance Needs	UV, abrasion, industrial chemicals	Salt spray, immersion, cathodic disbondment
Application Environment	Controlled conditions possible	Limited accessibility, high humidity, offshore wind constraints

4.3 Cost Considerations and Maintenance Requirements

Initial installation costs for offshore coatings were significantly higher due to:

- The use of high-performance coating systems
- Increased surface preparation standards
- Logistical challenges in transporting materials and equipment to offshore sites
- Labor cost surcharges due to personnel safety training and transport

Maintenance on offshore platforms was logistically difficult and costly, so durability and extended coating life were prioritized, even though initial material and application costs were significantly higher compared to onshore. Onshore maintenance occurred more frequently, typically every 8–15 years, while offshore coatings required maintenance only every 15–25 years or longer, as summarized in Table 2.

Table 2. *Cost Considerations and Maintenance Requirements for Onshore and Offshore Coatings*

Aspect	**Onshore**	**Offshore**
Material Cost	Low to moderate	High
Application Cost	Moderate	High
Maintenance Frequency	Every 8–15 years	Every 15–25 years or longer

4.4 Under-Film Corrosion and Failure Modes

Under-film corrosion had been a serious problem, especially in offshore systems, where small coating defects had allowed moisture to penetrate. Offshore environments had involved constant exposure to high levels of water vapor and salt contamination from airborne salt and immersion, which led to rapid corrosion under the coating. In contrast, onshore exposure to water vapor had been seasonal and salt contamination had mainly come from industrial pollution or ground chlorides. Typical failure modes offshore had included osmotic blistering, cathodic disbandment, and rapid under-film corrosion, resulting in a high to severe risk level, while onshore risks had generally been moderate, with issues such as coating chalking and adhesion loss. These differences were also summarized in Table 3.

Table 3. Risk Factors for Onshore and Offshore Environments

Risk Factor	**Onshore**	**Offshore**
Water vapor exposure	Seasonal/humidity-dependent	Constant/high
Salt contamination	Industrial pollution, ground chlorides	Airborne salt, immersion
Typical Failure Modes	Coating chalking, adhesion loss	Osmotic blistering, cathodic disbondment, rapid under film corrosion
Risk Level	Moderate	High to severe

To prevent under-film corrosion in offshore environments, barrier coatings needed to have very low water vapor transmission rates, strong adhesion, and resistance to osmotic blistering [36]. Techniques such as edge sealing, applying stripe coatings, and carefully controlling the curing process were crucial to eliminate weak spots that could allow corrosion to start [37].

4.5 Testing and Quality Assurance Differences

The quality control and inspection protocols for onshore and offshore coatings differed significantly due to environmental constraints and the criticality of failure. In offshore environments, inspections and certifications were usually required because of the critical safety risks involved with these structures [38]. On the other hand, onshore facilities often had more flexibility, with inspection requirements varying based on the level of operational risk [39].

The differences in coating approaches between onshore and offshore industrial settings boiled down to varying levels of exposure, risk tolerance, and maintenance accessibility. Offshore coatings had required more extensive surface preparation, multi-layer high-performance systems often including metallic layers, and stricter quality control following offshore standards. Onshore coatings, while still needing durability and safety, had involved simpler 2–3-layer systems, moderate initial costs, and easier maintenance access. Corrosion risk offshore was very high to extreme, leading to longer typical lifespans of 15–25+ years, whereas onshore risk was moderate to high with lifespans around 10–15 years. Under-film corrosion risk was critical offshore but manageable onshore. Table 4 provided a summary of these distinctions.

Table 4. *Summary Table – Onshore vs Offshore Coating Systems*

Criteria	Onshore	Offshore
Corrosion Risk	Moderate to high (C3–C5-I)	Very high to extreme (C5-M to CX)
Coating System Complexity	2-3 layers	3–5 layers, often metallic base
Typical Lifespan	10–15 years	15–25+ years
Initial Cost	Moderate	High
Maintenance Access	Easy to moderate	Difficult, weather-dependent
UFC Risk	Manageable	High (critical)
QC Requirements	Standard ISO	Strict offshore standards

5. COATING TECHNIQUES FOR INDUSTRIAL PIPING IN ONSHORE AND OFFSHORE ENVIRONMENTS

5.1 Coating Techniques for Onshore Piping

A typical onshore coating system included: a typical onshore coating system included a zinc phosphate primer, which provided good adhesion and basic corrosion resistance [40]. This was followed by a high-build epoxy intermediate coat that offered chemical resistance and acted as a moisture barrier [41]. Finally, a polyurethane or acrylic topcoat was applied to enhance weather resistance and improve the aesthetic appearance of the coated surface [42]. Application was generally conducted in controlled environments using airless spray equipment, which ensured uniform film build and efficient application. In certain instances, epoxy-based protective coatings like Fusion Bonded Epoxy were utilized on offshore pipelines or components that needed enhanced resistance to chemical exposure [43]. The preparation of surfaces typically involved abrasive blasting to eliminate rust, scale, and other contaminants, which helped promote effective adhesion of the coating material [44]. In some instances, solvent or alkaline cleaning was also used beforehand to eliminate oils, grease, and salt deposits [45]. After coating, the curing process was usually carried out in controlled environments, sometimes with the aid of heating systems.

5.2 Coating Techniques for Offshore Piping

The most widely used offshore coating systems include:

- Thermal Spray Aluminum (TSA) was a highly durable metallic coating that provided both barrier and sacrificial protection [46]. TSA was applied by flame spraying onto steel and was often sealed with an epoxy or silicone-based topcoat. Its use was widespread on risers, splash zones, and legs of offshore platforms, offering up to 30 years of maintenance-free service [47].

- 3-Layer Polyethylene and Polypropylene systems were primarily employed for subsea pipelines. These coatings consisted of a Fusion Bonded Epoxy primer, an adhesive layer, and a tough polyolefin outer jacket. They provided excellent resistance to mechanical damage, moisture ingress, and impact [48].

- Glass flake epoxies were reinforced with micronized glass flakes to increase barrier properties. They were frequently used on pipe exteriors exposed to salt spray and chemical spills [49].

- Field-applied heat shrink sleeves were used for weld joints, these

sleeves formed a tight, water-resistant seal and were compatible with various pipe coatings [50].

Coating application methods in offshore environments varied depending on the type of coating used. For example, thermal spray aluminium and glass flake coatings required specialized spray equipment to ensure proper application. In underwater areas, coatings were often applied by trained divers or robotic systems using materials specifically designed to bond to wet or submerged surfaces.

6. CONCLUSION

Protecting industrial piping systems involved much more than just preventing rust. Coatings played a critical role in maintaining system safety, reliability, and smooth operation, especially in harsh environments where failure was not an option. Whether a pipeline was installed on land or offshore, choosing the right coating system and applying it properly was essential to ensure it could withstand the specific demands it faced. Onshore pipelines generally allowed for simpler, more cost-effective coatings, benefiting from easier access and more controlled application conditions. However, this did not mean they were risk-free; cutting corners on surface preparation or using inappropriate coatings still led to damage, leaks, or costly downtime. Offshore pipelines, conversely, faced some of the harshest conditions—saltwater spray, constant moisture, temperature fluctuations, strong currents, and mechanical stresses. In these cases, coating systems had to be especially durable, often involving multiple layers or advanced materials such as thermal spray aluminium or glass flake coatings. These cases served as powerful reminders that coatings were not merely an afterthought but a vital part of pipeline design and long-term performance. When properly selected and applied, coating systems could add decades of life to pipelines while reducing maintenance needs, preventing failures, and ensuring safety. Ultimately, success depended on understanding the environment, following best practices, and treating protective coatings as an integral part of the engineering process rather than just a finishing layer.

REFERENCES

[1] Umar, H., Khanan, M. A., Ogbonnaya, C., Shiru, A. A., & Baba, A. (2021). Environmental and Socioeconomic Impacts of Pipeline Transport Interdiction in Niger Delta, Nigeria. *Heliyon*, *7*(5), e06999. https://doi.org/10.1016/j.heliyon.2021.e06999

[2] Wang, G., Cheng, Q., Zhao, W., Liao, Q., & Zhang, H. (2022). Review on The Transport Capacity Management of Oil and Gas Pipeline Network: Challenges and Opportunities of Future Pipeline Transport. *Energy Strategy Reviews*, *43*, 100933. https://doi.org/10.1016/j.esr.2022.100933

[3] Aghazadeh, K., & Attarnejad, R. (2024). Experimental Investigation of Desalination Pipeline System and Vapor Transportation by Temperature Difference Under Sub-Atmospheric Pressure. *Journal of Water Process Engineering*, *60*, 105133. https://doi.org/10.1016/j.jwpe.2024.105133

[4] Yeganeh, M., Heydarie, Y., Shahryari, Z., Asadi, N., Kahkesh, H., & Ramezanalizadeh, H. (2025). Corrosion Inhibitor of API Pipeline Steels: a Review. *Journal of Bio- and Tribo-Corrosion*, *11*(2). https://doi.org/10.1007/s40735-025-00965-2

[5] Shree Meenakshi, K. (2021). A Study of Corrosion Control in Pipelines. *Parıpex-Indian Journal of Research*, 48–49. https://doi.org/10.36106/paripex/4307062

[6] Hu, Z., Tariq, S., & Zayed, T. (2021). A Comprehensive Review of Acoustic Based Leak Localization Method in Pressurized Pipelines. *Mechanical Systems and Signal Processing*, *161*, 107994. https://doi.org/10.1016/j.ymssp.2021.107994

[7] Ervina Efzan, M. N., & Kesahvanveraragu, S. (2014). Review on Pipelines in Offshore Platform Processing System. *Applied Mechanics and Materials*, 695, 684 - 687. https://doi.org/10.4028/www.scientific.net/AMM.695.684

[8] Nassar, N. E. A. (2022). Corrosion in Marine and Offshore Steel Structures: Classification and Overview. *International Journal of Advanced Engineering Sciences and Applications*, *3*(1), 7–11. https://doi.org/10.47346/ijaesa.v3i1.80

[9] Desai, P. D., Pawar, C. B., Avhad, M. S., & More, A. P. (2022). Corrosion Inhibitors for Carbon Steel: A Review. *Vietnam Journal of Chemistry*, *61*(1), 15–42. https://doi.org/10.1002/vjch.202200111

[10] Jacques, L., Steve, D., & Alain, H. (2021). Cast Iron: A Historical and Green Material Worthy of Continuous Research. *International Journal of Technology*, *12*(6), 1123. https://doi.org/10.14716/ijtech.v12i6.5235

[11] Xie, Y., Chu, X., Ouyang, P., Jiang, L., Xing, J., Yao, H., & Zayed, T. (2024). A Mini Review on Coated Pipes: Materials, Manufacturing and Anti-Corrosion Protection. *Corrosion Engineering Science and Technology: The International Journal of Corrosion Processes and Corrosion Control*. https://doi.org/10.1177/1478422x241278895

[12] Ak, D., & Ad. P. (2015). Stainless Steel for Dairy and Food Industry: A review. *Journal of Material Science & Engineering*, *04*(05). https://doi.

org/10.4172/2169-0022.1000191

[13] Abdel-Ghany, M., Kharoup, O., & Yossef, N. (2022). Life Cycle Costing of Structures Fabricated from Carbon and Stainless Steel. *Journal of Engineering Research - Egypt*, 213–217. https://doi.org/10.21608/erjeng.2022.177208.1126

[14] Behrens, R. (2022). 2.2 Special Steels and Alloys for Industrial Use. *From Construction Materials to Technical Gases*, 123.

[15] Bhiogade, D. S. (2023). Ultra Supercritical Thermal Power Plant Material Advancements: A Review. *Journal of Alloys and Metallurgical Systems*, *3*, 100024. https://doi.org/10.1016/j.jalmes.2023.100024

[16] Aberle, D., & Agarwal, D. (2008). High Performance Corrosion Resistant Stainless Steels and Nickel Alloys for Oil & Gas Applications. *Corrosion*, 1–17. https://doi.org/10.5006/c2008-08085

[17] Kundig, K. J. A., & Weed, R. D. (2015). Copper and Copper alloys. *Mechanical Engineers' Handbook*, 1–111. https://doi.org/10.1002/9781118985960.meh104

[18] Zinkle, S. J. (2015). Applicability of Copper Alloys for DEMO High Heat Flux Components. *Physica Scripta*, *T167*, 014004. https://doi.org/10.1088/0031-8949/2015/t167/014004

[19] Hutton, B. L. (2024). The Evolution of Thermoplastics as a Solution to MIC and Oxidative Corrosion Issues. *Conference*, 1–14. https://doi.org/10.5006/c2024-20978

[20] Andrady, A. L., Pandey, K. K., & Heikkila, A. M. (2019). Interactive Effects of Solar UV Radiation and Climate Change on Material Damage. *Photochemical & Photobiological Sciences*, *18*(3), 804–825. https://doi.org/10.1039/c8pp90065e

[21] Blount, J. (2025). Ductile Iron vs Cast Iron Pipe: A Comparison of Physical Properties and Corrosion Resistance. *Conference*, 1–9. https://doi.org/10.5006/c2025-00252

[22] Grigg, N. S. (2017). Global Water Infrastructure: State of The Art Review. *International Journal of Water Resources Development*, *35*(2), 181–205. https://doi.org/10.1080/07900627.2017.1401919

[23] Yan, M., Sun, C., Xu, J., & Ke, W. (2014). Anoxic Corrosion Behavior of Pipeline Steel in Acidic Soils. *Industrial & Engineering Chemistry Research*, *53*(45), 17615–17624. https://doi.org/10.1021/ie502728a

[24] Qamar, S. Z., Pervez, T., & Al-Jahwari, F. (2023). Integrity Assessment of High-Performance PVC Pipes for Thermal Wells. Polymers, 15(17), 3593. https://doi.org/10.3390/polym15173593

[25] Tache, I. A., & Tache, C. (2020). Coatings & Linings for Oil & Gas Pipelines – The Most Effective Method of Corrosion Protection for Aged Pipelines. *MATEC Web of Conferences*, *305*, 16. https://doi.org/10.1051/matecconf/202030500016

[26] Dahl, L. (1992). Corrosion in Flue Gas Desulfurization Plants and Other Low Temperature Equipment. *Materials and Corrosion*, *43*(6), 298–304.

https://doi.org/10.1002/maco.19920430610

[27] Kangas, P., & Chai, G. C. (2013). Use of Advanced Austenitic and Duplex Stainless Steels for Applications in Oil & Gas and Process Industry. *Advanced Materials Research*, *794*, 645–669. https://doi.org/10.4028/www.scientific.net/amr.794.645

[28] Alfattah, M., Arwati, I. G. A., & Majlan, E. H. (2024). A Review Analysis of Corrosion Rate on Stainless Steel Pipe in Sea Water Media. *Sinergi*, *28*(3), 567. https://doi.org/10.22441/sinergi.2024.3.013

[29] Mehdi, M. S., & Al-Dossary, A. K. (2013). Thermoplastic Lined Pipework for Corrosive Applications. *Corrosion*, 1–7. https://doi.org/10.5006/c2013-02197

[30] Malikasri, N. B. R., Kishore, K., Arora, K. S., & Mahobia, G. S. (2024). Failure Mechanisms of Blast Furnace Tuyeres and Mitigation Strategies: A Comprehensive Review. *Engineering Failure Analysis*, *167*, 108968. https://doi.org/10.1016/j.engfailanal.2024.108968

[31] Xie, X., Chi, C., Yu, H., Yu, Q., Dong, J., Chen, M., & Zhao, S. (2010). Results from Structural Stability Studies of Advanced Heat-Resistant Steels and Alloys for Fossil Power Plants in China. *Advances in Materials Technology for Fossil Power Plants: 84659*, 30–52. https://doi.org/10.31399/asm.cp.am-epri-2010p0030

[32] Popoola, A., Olorunniwo, O., & Ige, O. (2014). Corrosion Resistance Through the Application of Anti- Corrosion Coatings. In *InTech eBooks*. https://doi.org/10.5772/57420

[33] López-Ortega, A., Bayón, R., & Arana, J. L. (2019). Evaluation of Protective Coatings for High-Corrosivity Category Atmospheres in Offshore Applications. *Materials*, *12*(8), 1325. https://doi.org/10.3390/ma12081325

[34] Xia, R., Jia, C., & Garbatov, Y. (2024). Deterioration of Marine Offshore Structures and Subsea Installations Subjected to Severely Corrosive Environment: A review. *Materials and Corrosion*. https://doi.org/10.1002/maco.202314050

[35] Grinon-Echaniz, R., Paul, S., Thornton, R., Refait, P., Jeannin, M., & Rodriguez, A. (2021). Prediction of Thermal Spray Coatings Performance in Marine Environments by Combination of Laboratory and Field Tests. *Coatings*, *11*(3), 320. https://doi.org/10.3390/coatings11030320

[36] Chung, K., Pizanowski, T. E., Lo, F., & Chung, A. (2024). Field Applicable PVDF Corrosion Protection Coating for Marine Assets. *Conference*, 1–15. https://doi.org/10.5006/c2024-20848

[37] Ingle, M., Slebodnick, P., Martin, J., Ellor, J., & Cassidy, P. (2011). High Solids Coatings Performance and Service History. *Corrosion*, 1–8. https://doi.org/10.5006/c2011-11421

[38] Mitchell, M. J., Claydon, D., & Ward, D. (2005). A Critical Review of Current Performance Tests for Offshore Anti-Corrosive Coatings. *Corrosion*, 1–17. https://doi.org/10.5006/c2005-05021

[39] Martin, A. T. (2003). Decommissioning of International Petroleum Facilities

Evolving Standards and Key Issues. Oil, Gas & Energy Law Journal, 1.

[40] Romagnoli, R., & Vetere, V. F. (1995). Heterogeneous Reaction between Steel and Zinc Phosphate. *Corrosion*, *51*(2), 116–123. https://doi.org/10.5006/1.3293583

[41] Yang, X., Zhang, T., Wang, H., & Hou, B. (2011). A New Solvent-Free Super High Build Epoxy Coating Evaluated by Marine Corrosion Simulation Apparatus. *Materials and Corrosion*, *63*(4), 328–332. https://doi.org/10.1002/maco.201005841

[42] Squiller, E. P., & Best, K. E. (2008). 2-Component Polyurethane Topcoats – Formulating Variables Affecting Weathering Performance. Paint and Coatings Expo (PACE) 2008.

[43] Zamanzadeh, M., & Xu, H. (2016). Fusion Bonded Epoxy Coatings (FBE) and Disbondment. *Corrosion*, 1–11. https://doi.org/10.5006/c2016-07246

[44] Santos, I. S. D., De Carvalho, L. J., Reznik, L. Y., & Brasil, S. L. D. C. (2020). Anti-Corrosive Properties of Two Epoxy Primer Systems Applied to Steel Surfaces Prepared with Various Mechanical Abrasive Treatments. *Journal of Adhesion Science and Technology*, *34*(22), 2467–2483. https://doi.org/10.1080/01694243.2020.1767476

[45] Westray, W. K. (2018). Metal Cleaning. In *Routledge eBooks*, 427–437. https://doi.org/10.1201/9781315136691-17

[46] Ryen, A., Johnsen, R., Iannuzzi, M., & Artun, L. (2018). Cathodic Protection by Distributed Sacrificial Anodes – Performance at Elevated Temperature and in Mud. *Corrosion*, 1–15. https://doi.org/10.5006/c2018-11106

[47] Fischer, K. P., Rosbrook, T., Thomason, W. H., & Murali, J. (1994). Performance of Thermal Sprayed Aluminium Coatings in The Splash Zone and For Riser Service. *Corrosion*, 1–21. https://doi.org/10.5006/c1994-94499

[48] Mallozzi, M., & Perez, M. (2010). A New 3LPP Offshore Field Joint Coating. *Corrosion*, 1–9. https://doi.org/10.5006/c2010-10010

[49] Alagoz, E., & Selver, E. (2024). Glass Flakes for Enhancing Mechanical Properties of Glass/Epoxy Composites. *Proceedings of the Institution of Mechanical Engineers Part L Journal of Materials Design and Applications*, *238*(8), 1438–1456. https://doi.org/10.1177/14644207231224784

[50] Sand, K., Sincovich, G., Simpson, B., Cheshire, B., & Patton, C. (2025). Protecting Your Asset: The Cooperation Between Cathodic Protection Systems and Pipeline Coatings. *Conference*, 1–13. https://doi.org/10.5006/c2025-00411

Chapter 2

INNOVATIONS IN PHARMACEUTICAL PROCESS MODELING AND UNRAVELING COMPLEXITIES OF PARTICLE PROCESS[1]

Mohannad Ayman Natheer SABHA[2]

Fatma İrem ŞAHİN[3]

Nil ACARALI[4]

1 *For correspondence: Prof.Dr. Nil ACARALI; nbaran@yildiz.edu.tr
2 Yildiz Technical University, Department of Chemical Engineering, 34220, Esenler-Istanbul, Türkiye.
0009-0003-8817-8208
3 Yildiz Technical University, Department of Chemical Engineering, 34220, Esenler-Istanbul, Türkiye.
0000-0001-7670-8871
4 Yildiz Technical University, Department of Chemical Engineering, 34220, Esenler-Istanbul, Türkiye.
0000-0003-4618-1540

1. INTRODUCTION

The pharmaceutical sector had long been driven toward the adoption of increasingly effective procedures because of regulatory frameworks in conjunction with economic, environmental, health, and safety requirements [1–3]. Such a transformation was regarded not merely as a desirable trend but as an essential adaptation to ensure sustainability, enhance competitiveness, and maintain compliance within a highly regulated industrial environment. Although the production of pharmaceuticals had historically been accompanied by considerable technical and organizational challenges, the sector was nevertheless acknowledged to have derived substantial benefits from these advancements [4]. Beyond its direct contributions to drug development, the pharmaceutical industry was also recognized as exerting a profound and lasting influence on global healthcare practices. It had consequently emerged as one of the most influential agents of social change and had become a key determinant of institutional structures and public health outcomes, particularly within industrialized societies [5].

Over the past decades, the industry had consistently maintained its position as one of the most research-intensive sectors worldwide, generating a continuous pipeline of novel therapeutic agents. These innovations were not only instrumental in improving quality of life but also contributed significantly to the global reduction of mortality and morbidity rates [6]. The expansion of the market for generic pharmaceutical products had been facilitated by the strategic efforts of domestic producers. By reinforcing their financial capacities, establishing export-oriented logistics systems, and organizing retail networks for international distribution, these producers had succeeded in gaining competitive advantages while simultaneously contributing to the diversification and resilience of global supply chains [7]. Moreover, the discovery and subsequent large-scale development of broad-spectrum antibiotics such as synthetic penicillin, streptomycin, and tetracycline had been recognized as a milestone achievement in the historical progression of therapeutic innovation [8].

Within continuously evolving industrial landscape, chemical and biochemical engineers had assumed a pivotal role in the conceptualization, design, and refinement of processing and purification procedures. Specialized expertise in areas such as modelling, process design, and scale-up was considered indispensable in bridging the gap between laboratory-scale discoveries and full-scale industrial manufacturing. By virtue of these contributions, greater efficiency had been achieved, while product consistency and quality in pharmaceutical production were more reliably assured [9]. Among the most significant advancements in recent years,

the adoption of continuous production methods had been identified as a transformative shift in pharmaceutical manufacturing practices. Approaches were valued for capacity to broaden operational flexibility and enable more stringent quality control, particularly when contrasted with conventional batch production systems [10].

Traditional batch-based processes, due to inherently sequential character, were often constrained by prolonged cycle times and limited adaptability to rapidly changing market demands. In contrast, continuous manufacturing had been shown to facilitate uninterrupted operation, reduce idle periods, and minimize inter-batch variability. Advantages collectively contributed to stronger and more consistent alignment with regulatory expectations. Furthermore, continuous systems were regarded as being particularly responsive to supply shortages and public health emergencies, since production capacity could be expanded through extended operating times or the integration of parallel lines, thereby avoiding the considerable costs and delays associated with the construction of entirely new facilities. Despite these advancements, it was observed that modelling practices within the sector had not consistently reached a comparable level of maturity. A substantial number of models employed in earlier investigations lacked rigorous mathematical formulation and were primarily qualitative in orientation, which restricted their predictive reliability under diverse process conditions [11, 12].

These limitations curtailed the extent to which manufacturers could fully leverage model-based decision-making approaches, particularly in complex solid dosage processes, where precise control and optimization were critically important. Main challenges and improvement areas in pharmaceutical manufacturing were shown in Table 1.

Table 1. *Key challenges and potential areas for improvement in pharmaceutical manufacturing*

Area	**Challenges**	**Improvement Possibilities**
Raw Material Quality	Variability, purity issues	Supply chain control, standardization
Process Parameters	Complex interdependencies, sensitivity	Process optimization, precise monitoring
Regulation	Strict compliance requirements	Standardized procedures for conformity
Production Method	Limitations of batch manufacturing	Flexibility and quality increase through continuous production
Modelling	Mostly qualitative or incomplete models	Combination of mechanical and statistical methods

Nevertheless, past developments had progressively conferred upon process modelling a more prominent and influential position within the broad spectrum of engineering tasks associated with pharmaceutical production. Over time, the steady advancement of computational methodologies and the refinement of numerical techniques, when combined with the increasing accessibility of industrial-scale data, had collectively enabled the construction of models that were both more robust in structure and more quantitative in their predictive capacity. Through these converging improvements, process modelling had been elevated from a supplementary analytical approach to an indispensable component of modern pharmaceutical engineering practice. It had thereby been recognized as essential not only for process design and scale-up but also for the systematic execution of safety analyses, the comprehensive evaluation of plant operability, and the holistic optimization of pharmaceutical manufacturing operations [13].

2. MODELLING METHODS USED IN PHARMACEUTICAL MANUFACTURING

The discrete element method (DEM) had historically been recognized as the most widely applied modelling technique for the investigation of granular materials in pharmaceutical processes [14]. Classification of several modelling approaches were shown in Figure 1. Hybrid approaches that combined different modelling paradigms, had also been employed to capture complementary aspects of process behaviour. DEM had demonstrated considerable reliability as a predictive tool and had consequently been applied across a wide variety of pharmaceutical operations. These applications included powder blending, powder conveyance, milling, granulation, as well as the analysis of tablet motion during film-coating procedures. Through its implementation in these critical stages of production, DEM had generated valuable insights into the dynamic behaviour of particulate systems and had thereby contributed to an enhanced understanding of how critical quality attributes were affected throughout pharmaceutical manufacturing [15, 16].

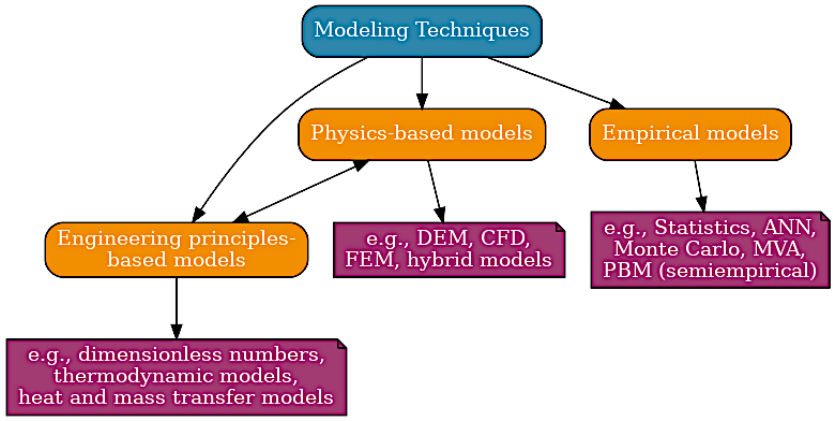

Figure 1. *Classification of several modelling approaches [14]*

Methodologically, DEM had been based on Newton's equations of motion, whereby the trajectories of individual particles were calculated through the numerical integration of the forces acting upon them over discrete time steps. From calculations, the instantaneous velocity and position of each particle could be determined with a high degree of resolution [14, 17].

The range of forces incorporated into DEM simulations typically encompassed gravitational, contact, cohesive, and fluid–particle interactions, all of which were indispensable for the accurate representation of realistic process conditions. This capacity to reproduce particle-scale interactions had rendered DEM particularly well suited to pharmaceutical operations in which powders and granules were frequently handled, given that the uniformity and overall quality of the final product were strongly dependent on the collective behaviour of individual particles. Moreover, by enabling the exploration of phenomena such as segregation, agglomeration, and flowability at the particle scale, DEM had offered researchers and engineers a powerful means of identifying potential sources of variability within manufacturing systems. It had facilitated the design and implementation of more consistent, reliable, and efficient pharmaceutical processes. Through such contributions, DEM had ultimately been recognized not only as a predictive modelling tool but also as a strategic instrument for advancing the scientific understanding and technological optimization of particulate-based pharmaceutical manufacturing [18].

Computational modelling had also been employed in a range of additional pharmaceutical operations, one notable example being the prediction of nasal spray deposition patterns, in which the accurate representa-

tion of particle flow and distribution was of critical importance [19].

Computational approaches had provided a means of simulating the complex aerodynamics of spray droplets as they interacted with the anatomical geometry of the nasal cavity. By enabling the visualization and quantification of deposition sites, such models had contributed to a more precise understanding of drug delivery efficiency and therapeutic effectiveness. The efficiency and applicability of computational modelling for nasal spray performance were illustrated in Figure 2, where the capability of these methods to replicate realistic distribution patterns had been demonstrated.

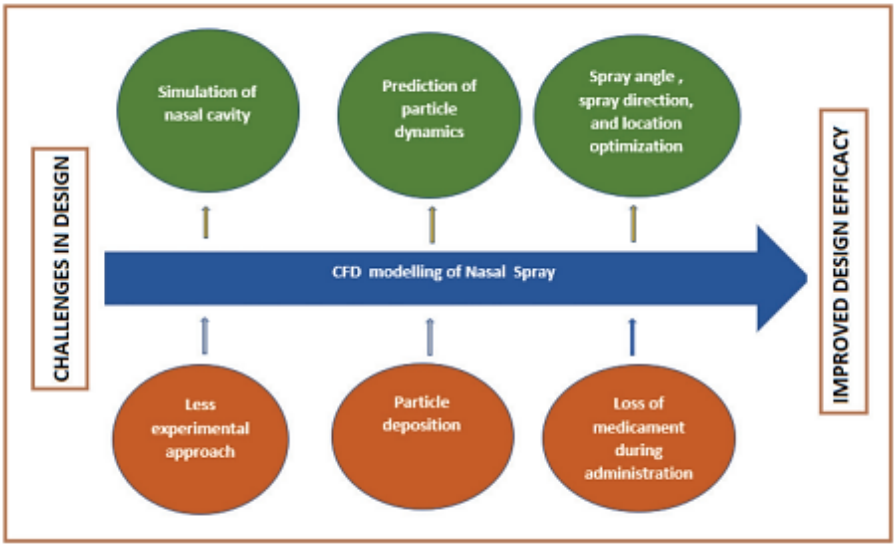

Figure 2. *The efficiency of computational modelling on nasal spray [19]*

In addition to DEM, the discrete particle contact (DPC) model had also been employed with increasing frequency in several studies. This method had demonstrated its effectiveness by providing reliable predictive outcomes while simultaneously requiring fewer computational resources, which rendered it a more resource-efficient approach compared to alternative modelling techniques. Owing to these advantages, the DPC model had been regarded as a trustworthy and practical option for research within the field of pharmaceutical process modelling [20]. Modelling methods used in pharmaceutical manufacturing was shown in Table 2.

Table 2. *Modelling methods used in pharmaceutical manufacturing*

Method	**Application Areas**	**Advantages**	**Limitations**
DEM (Discrete Element Method)	Powder blending, granulation, milling, tablet coating	Accurate particle-level results	High computational cost
FEM (Finite Element Method)	Stress/structure analysis, equipment design	Strong in mechanical/structural analysis	Not suitable for powder flows
CFD (Computational Fluid Dynamics)	Fluid flows, spray drying, coating	Captures flow behaviour effectively	Relies on simplified assumptions
Hybrid Approaches	Combination of mechanical + statistical	Utilizes strengths of both methods	Requires large datasets

The emergence of hybrid modelling strategies, in which statistical regression techniques were systematically combined with material balance frameworks, had represented a particularly important advancement in the discipline. These methods had been motivated by the recognition that neither purely mechanistic models nor purely statistical approaches could, in isolation, provide sufficiently accurate or generalizable representations of complex pharmaceutical processes. Mechanistic models, while offering strong theoretical grounding and physical interpretability, were often constrained by simplifying assumptions and the unavailability of complete physicochemical data. Conversely, statistical models could capture empirical correlations directly from experimental datasets, but they frequently lacked explanatory power and could struggle to predict system behaviour outside of the calibration range. By integrating the complementary strengths of both approaches while minimizing their respective limitations, hybrid methods had contributed to the establishment of more robust modelling practices. In these frameworks, mechanistic equations describing mass and energy balances, reaction kinetics, or transport phenomena were systematically coupled with regression-based sub-models that accounted for empirical variability, process noise, or unmodeled interactions. The combined architecture allowed the models to retain physical meaning while simultaneously achieving high predictive accuracy. This balance had made hybrid methods particularly appealing in pharmaceutical contexts, where both scientific understanding and regulatory validation demanded a careful equilibrium between transparency and

performance. As a result, the scope and applicability of predictive tools available to pharmaceutical engineers had been significantly broadened. Hybrid models had supported the development of more comprehensive and reliable simulations of pharmaceutical manufacturing processes, enabling the exploration of phenomena such as powder blending uniformity, granulation kinetics, drying behaviour, crystallization dynamics, and even downstream operations such as coating and tableting [21] (Figure 3).

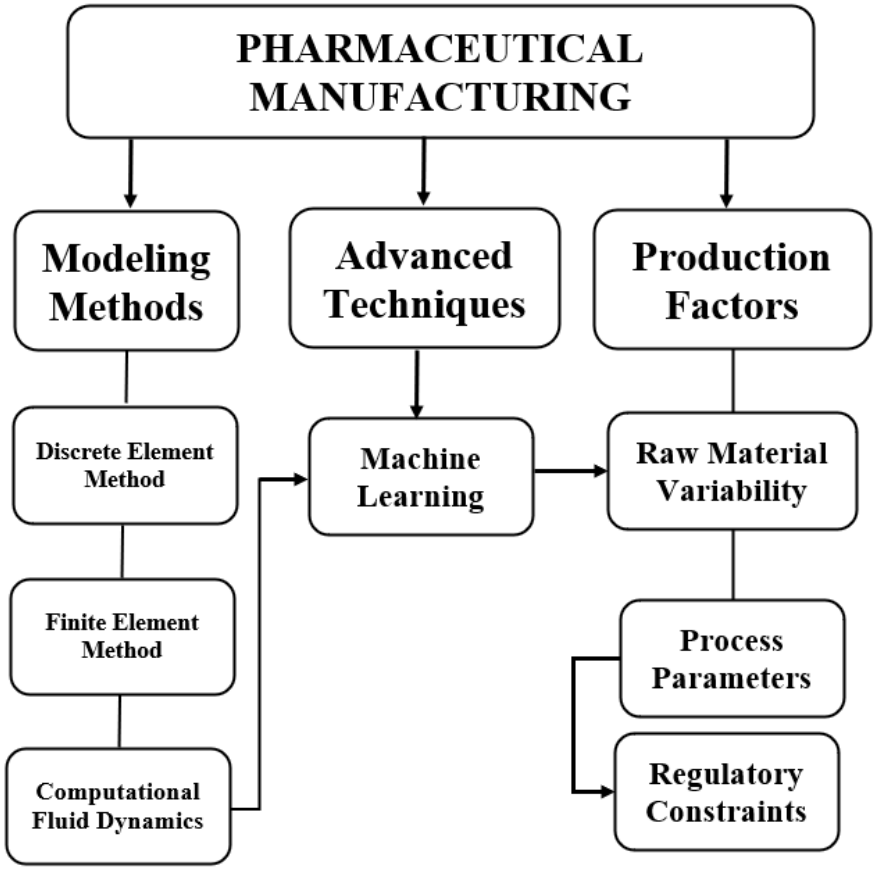

Figure 3. *Key modelling methods and influencing factors in pharmaceutical manufacturing [21]*

3. PROCESS MODELLING AND SIMULATION FOR SPECIFIC DRUGS

In process modelling, plug flow reactors (PFRs) were connected in series to enable the production of ibuprofen and it had been designed to serve as a representative case study for the application of continuous processing strategies in pharmaceutical manufacturing. The specific reactor configuration had been deliberately selected with the intention of demonstrating not only the technical feasibility but also the practical applicability of continuous operation for an active pharmaceutical ingredient (API) that had traditionally been manufactured through conventional batch operations. By employing this sequential PFR arrangement, researchers were able to replicate essential stages of the synthesis pathway while simultaneously achieving higher levels of conversion efficiency compared to a single reactor unit. In doing so, the configuration provided a clear and instructive contrast between the operational principles of continuous and batch-based systems, thereby highlighting the potential advantages of continuous manufacturing approaches in terms of throughput, process control, and scalability [22]. Beyond its comparative function, the system also offered a useful framework for exploring how reactor design choices could influence critical performance parameters such as residence time distribution, conversion yield, and thermal stability. The modularity of the series configuration made it possible to incrementally increase conversion across successive reactor units while maintaining a manageable operational footprint. This characteristic had been recognized as a significant advantage in pharmaceutical manufacturing, where process intensification and facility efficiency are of increasing importance. The design of the reactors had been conducted under a set of simplifying assumptions to facilitate modelling and simulation. It had been presumed that the reacting system behaved as a perfect solution, thereby always ensuring complete homogeneity of the mixture. Under this assumption, molecular-level mixing was considered instantaneous, and concentration profiles were represented as uniform across the entire cross-section of the reactor. To reduce the complexity of the mathematical treatment, both radial concentration gradients and radial or axial temperature gradients had been neglected, resulting in an isothermal operational framework [23]. Within this framework, heat generation from exothermic reactions or losses due to heat transfer through reactor walls were disregarded, thus enabling a more tractable analysis.

Furthermore, possible phase changes had not been considered within the system, and constant values had been assumed for thermophysical properties such as heat capacities and reaction enthalpies across each reactor unit. These assumptions collectively allowed the process to be

represented according to the principles of ideal plug flow behaviour, in which all fluid elements travel through the reactor at the same velocity and experience identical residence times. Such an idealized description enabled tractable kinetic modelling, simplified numerical computation, and straightforward simulation of reaction dynamics, thereby providing a strong foundation for examining the feasibility of continuous ibuprofen production (Figure 4).

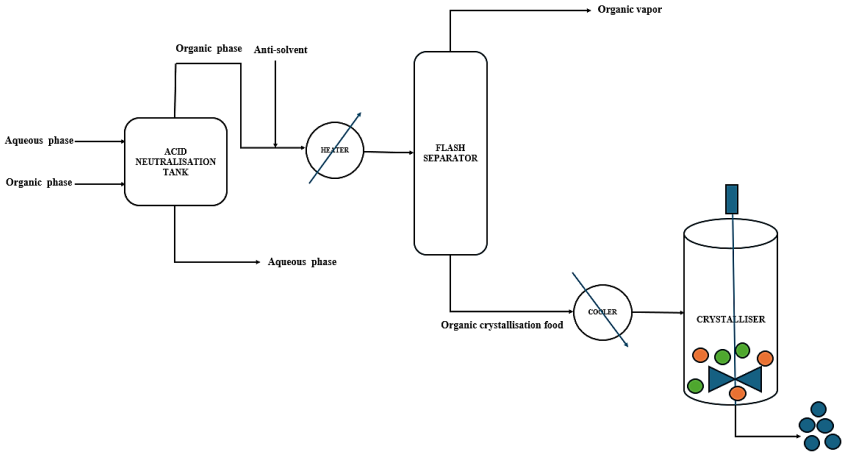

Figure 4. *Generalised of the continuous separation system [23]*

By connecting the three reactors in series, conversion had been progressively enhanced, with each subsequent stage contributing incrementally to the overall yield of ibuprofen. The simplified modelling framework had made it possible to estimate reaction rates, assess reactor performance, and predict conversion efficiencies under steady-state conditions. Although such simplifications had inevitably constrained the model's ability to capture the full complexity of industrial-scale operation, they nevertheless provided a workable and analytically useful foundation for evaluating continuous ibuprofen synthesis and for drawing comparisons with conventional batch-based production methods.

It had, however, been acknowledged that these assumptions also imposed certain limitations on the accuracy of the model in reflecting real-world manufacturing conditions. Potential improvements were identified in future work, including the incorporation of non-ideal behaviours such as heat and mass transfer limitations, phase equilibria effects, and spatial gradients in both concentration and temperature. By integrating these more realistic considerations, process simulations could have attained higher predictive accuracy, thereby offering stronger and more reliable support for the large-scale implementation of continuous ibu-

profen production. Moreover, additional case studies concerning specific active pharmaceutical ingredients had illustrated the applicability and limitations of process modelling and simulation in diverse continuous or semi-continuous production contexts. For example, continuous crystallization of atorvastatin calcium had been investigated using hybrid reaction-crystallization-spherical agglomeration-filtration-drying process modules, where integrated modelling enabled evaluation of yield, crystal size distribution, and polymorphic form control under continuous manufacturing conditions [24].

Another case was the modelling and techno-economic optimisation of a Continuous Oscillatory Baffled Crystalliser (COBC) for paracetamol crystallization. In that study, nonlinear programming techniques had been applied to design and operate the continuous crystallizer, determining optimal seed mass loading, antisolvent ratio, and crystallizer volume to balance yield, crystal size, and cost [25]. These examples underscored that when moving beyond small-scale or idealised reactors, the incorporation of downstream operations, along with realistic mass and heat transfer constraints, became essential for models to produce reliable predictions for industrial scale.

4. ANALYSIS AND EVALUATION

The principles underlying modern process methodologies had not originally emerged within the pharmaceutical industry but had instead been adopted and adapted from other technologically advanced sectors, including petrochemicals, polymers, and energy [26]. These sectors had historically pioneered the development of advanced modelling, optimization, and control strategies, primarily as a response to the economic and safety demands associated with large-scale industrial operations. When such approaches were subsequently transferred into pharmaceutical production, they did not enter as neutral tools but required significant adjustment to accommodate the unique regulatory, physicochemical, and organizational contexts of pharmaceutical manufacturing. This transition, while promising in terms of efficiency gains and improved process reliability, had presented the sector with a series of complex and multifaceted challenges that spanned scientific, technical, and regulatory domains [27].

Among the primary reasons for these challenges was the continuum duality of particulate materials. This concept emphasized that microscopic particle-level interactions—such as collision, adhesion, or breakage—could exert a decisive influence on the macroscopic behaviour of bulk particulate flows. In practice, this meant that even slight variations

in particle size, shape, or surface properties could lead to disproportionate changes in flowability, segregation, and compaction performance. As a result, it had proven particularly difficult to develop constitutive models capable of reliably predicting how granular systems respond to applied stresses and strains across different process scales [10].

In addition to these scientific barriers, the highly regulated nature of pharmaceutical manufacturing added further layers of complexity. The sector operated under stringent requirements imposed by agencies such as the FDA and EMA, which demanded precise control, traceability, and validation of every stage of production. Coupled with this was the considerable diversity of physicochemical properties associated with active pharmaceutical ingredients (APIs)—ranging from hygroscopic powders to thermally sensitive compounds—which made the modelling and simulation of solids-based processes particularly challenging [28].

One of the most notable breakthroughs had been the application of discrete element method (DEM) simulations, which had demonstrated a remarkable capacity to capture detailed and accurate representations of particle-scale phenomena. Unlike continuum-based models, DEM provided a bottom-up framework in which the behaviour of individual particles could be simulated under different process conditions. These simulations offered valuable insights into critical pharmaceutical operations such as powder mixing, segregation, compaction, tableting, and flow dynamics within hoppers or feeders [26, 29].

By enabling such a level of analysis, DEM tools had supported both researchers and engineers in improving their understanding of complex process dynamics and in formulating more robust and reliable strategies for pharmaceutical manufacturing. Importantly, the benefits extended beyond traditional unit operations. Simultaneously, novel research fields such as advanced drug delivery systems and nanomedicine had emerged as highly dynamic and rapidly evolving domains of modern pharmaceutical science. These areas had attracted significant interest from both academic researchers and industrial stakeholders due to their potential to substantially enhance therapeutic efficiency, minimize side effects, and enable the development of innovative treatment modalities tailored to patient-specific needs [30, 31]. Nevertheless, despite their promise, effective implementation of these innovations had been recognized as dependent on extensive experimental validation and comprehensive clinical trials, which were considered indispensable for overcoming current barriers and confirming the safety, reproducibility, and efficacy of such systems [32].

Looking forward, future progress had been anticipated through the

systematic integration of advanced modelling and analytical techniques into pharmaceutical development pipelines. Such integration was expected to enhance the predictive capability of treatment outcome simulations, reduce reliance on trial-and-error experimentation, and support the optimization of pharmaceutical interventions under varying process conditions. By coupling rigorous process modelling with carefully designed clinical research, it was envisaged that the pharmaceutical sector would be able to address many of the persistent challenges that had constrained progress to date [33].

5. CONCLUSION

This review had explored the multifaceted domain of pharmaceutical manufacturing by providing a comprehensive examination of the principal factors that influenced production processes. A systematic discussion had been carried out on the inherent complexities and challenges associated with modelling pharmaceutical operations, including variability in raw materials, fluctuations in process parameters, and the constraints imposed by stringent regulatory requirements. Beyond merely identifying these limitations, the review had also highlighted the opportunities that could be leveraged to improve process understanding, operational efficiency, and overall robustness through the application of advanced technological interventions.

Emphasis had been placed on the transformative potential of emerging tools such as machine learning and artificial intelligence, which had demonstrated considerable promise in enhancing modelling accuracy, streamlining manufacturing workflows, and supporting the consistent attainment of higher product quality. These innovations had further been recognized for their ability to integrate seamlessly with existing engineering methodologies, thereby establishing hybrid, data-driven frameworks that provided valuable guidance for both research and industrial implementation.

The investigation had revealed that pharmaceutical process modelling remained fundamentally complex due to the combined effects of heterogeneous material properties, multiscale process dynamics, and evolving regulatory standards. Nevertheless, simulation technologies and advanced modelling approaches had been identified as promising avenues for optimization, particularly when supported by predictive analytics, artificial intelligence, and machine learning. Through such techniques, critical process parameters could be more effectively optimized, while manufacturing outcomes could be predicted with greater reliability.

Ultimately, it had been concluded that the pharmaceutical industry

could maximize the efficiency of production processes, strengthen product quality, and improve patient safety by acknowledging existing challenges, addressing data availability and integrity issues, ensuring adherence to regulatory frameworks, and embracing technological advancements. Moreover, the cultivation of collaborative efforts between academia, industry, and regulatory agencies had been emphasized as essential for advancing pharmaceutical manufacturing practices. By integrating traditional process engineering with modern data-driven tools, the sector was expected to establish a more resilient, efficient, and patient-oriented production paradigm capable of meeting future healthcare demands.

REFERENCES

[1] Domokos, A., Nagy, B., Szilágyi, B., Marosi, G., & Nagy, Z. K. (2021). Integrated continuous pharmaceutical technologies—A review. Organic Process Research & Development, 25(4), 721–739.

[2] Russell, A., Strong, J., Garner, S., Ketterhagen, W. R., Long, M. A., & Capece, M. (2022). Direct compaction drug product process modeling. AAPS PharmSciTech, 23(1), 67, 1-28.

[3] Uhlemann, J., Diedam, H., Hoheisel, W., Schikarski, T., & Peukert, W. (2021). Modeling and simulation of process technology for nanoparticulate drug formulations—A Particle Technology Perspective. Pharmaceutics, 13(1), 22, 1-25.

[4] Benyahia, B., Lakerveld, R., & Barton, P. I. (2012). A Plant-Wide dynamic model of a continuous pharmaceutical process. Industrial & Engineering Chemistry Research, 51(47), 15393–15412.

[5] Sismondo, S. (2015). Pharmaceutical industry: Political economies of drugs and knowledge. In International Encyclopedia of the Social & Behavioral Sciences. Elsevier, 6-10.

[6] Scherer F. M. (2000). The pharmaceutical industry, Handbook of Health Economics, Ch. 25, 1297–1336.

[7] Kisa, A. (2006). Analysis of the pharmaceuticals market and its technological development in Turkey. International Journal of Technology Assessment in Health Care, 22(4), 537–542.

[8] Grabowski, H. G. (2011). The evolution of the pharmaceutical industry over the past 50 years: a personal reflection. International Journal of the Economics of Business, 18(2), 161–176.

[9] Ende, D. J. A., & Ende, M. T. A. (2019). Chemical Engineering in The Pharmaceutical Industry. In John Wiley & Sons, Inc. eBooks, 1–17.

[10] Lee, S. L., O'Connor, T., Yang, X., Cruz, C. N., Chatterjee, S., Madurawe, R. D., Moore, C., Yu, L. X., & Woodcock, J. (2015). Modernizing pharmaceutical manufacturing: from batch to continuous production. Journal of Pharmaceutical Innovation, 10(3), 191–199.

[11] Jana, A. K. (2011). Steady-state process simulation. In Chemical Process Modelling and Computer Simulation (2nd ed., pp. 45–76). New Delhi: PHI Learning Pvt. Ltd.

[12] Ingham, J., Dunn, I. J., Heinzle, E., Přenosil, J. E., & Snape, J. B. (2007). Batch reactors. In Chemical Engineering Dynamics: An Introduction to Modelling and Computer Simulation (3rd ed., pp. 45–82). Wiley-VCH. ISBN: 9783527316786.

[13] Pantelides, C. C. (2001). New challenges and opportunities for process modelling. In Computer-aided chemical engineering, 34th European Symposium of the Working Party on Computer Aided Process Engineering, 15-22.

[14] Pandey, P., Bharadwaj, R., & Chen, X. (2017). Modelling of drug product

manufacturing processes in the pharmaceutical industry. In Elsevier eBooks, 1–13.

[15] Ketterhagen, W. R., Ende, M. T. A., & Hancock, B. C. (2009). Process modelling in the pharmaceutical industry using the discrete element method. Journal of Pharmaceutical Sciences, 98(2), 442–470.

[16] Afrasiabi, M., & Bambach, M. (2023). Modelling and simulation of metal additive manufacturing processes with particle methods: A review. Virtual and Physical Prototyping, 18(1), 1-37.

[17] Rantanen, J., & Khinast, J. G. (2015). The future of pharmaceutical manufacturing sciences. Journal of Pharmaceutical Sciences, 104(11), 3612–3638.

[18] Yeom, S. B., Ha, E., Kim, M., Jeong, S. H., Hwang, S. J., & Choi, D. H. (2019). Application of the discrete element method for manufacturing process simulation in the pharmaceutical industry. Pharmaceutics, 11(8), 414, 1-51.

[19] Lavanya, N., & Bhattacharyya, S. (2021). Computational fluid dynamics-the futuristic innovation in pharmaceutical industry. Indian Journal of Pharmaceutical Education and Research, 55(4), 930–938.

[20] Partheniadis, I., Terzi, V. G., & Nikolakakis, I. (2022). Finite element analysis and modelling in pharmaceutical tableting. Pharmaceutics, 14(3), 673, 1-32.

[21] Tsopanoglou, A., & Del Val, I. J. (2021). Moving towards an era of hybrid modelling: advantages and challenges of coupling mechanistic and data-driven models for upstream pharmaceutical bioprocesses. Current Opinion in Chemical Engineering, 32, 100691.

[22] Bogdan, A. R., Poe, S. L., Kubis, D. C., Broadwater, S. J., & McQuade, D. T. (2009). The continuous-flow synthesis of ibuprofen. Angewandte Chemie International Edition, 48(45), 8547–8550.

[23] Jolliffe, H. G., & Gerogiorgis, D. I. (2015). Process modelling and simulation for continuous pharmaceutical manufacturing of ibuprofen. Chemical Engineering Research & Design, 97, 175–191.

[24] Parvaresh, R., & Nagy, Z. K. (2024). Process intensification via end-to-end continuous manufacturing of atorvastatin calcium using an integrated, modular reaction-crystallization-spherical agglomeration-filtration-drying process. Organic Process Research & Development, 28(7), 2906–2918.

[25] Jolliffe, H. G., & Gerogiorgis, D. I. (2018). Process modelling, design and technoeconomic evaluation for continuous paracetamol crystallisation. Computers & Chemical Engineering, 103, 224–235.

[26] Rantanen, J., & Khinast, J. G. (2015). The future of pharmaceutical manufacturing sciences. Journal of Pharmaceutical Sciences, 104(11), 3612–3638.

[27] Rogers, A., & Ierapetritou, M. G. (2014). Challenges and opportunities in pharmaceutical manufacturing modelling and optimization. In Computer-

aided chemical engineering, 144–149.

[28] McKenzie, P., Kiang, S., Tom, J. W., Rubin, A. D., & Futran, M. (2006). Can pharmaceutical process development become high tech? Aiche Journal, 52(12), 3990–3994.

[29] Rogers, A., Hashemi, A., & Ierapetritou, M. (2013). Modeling of particulate processes for the continuous manufacture of solid-based pharmaceutical dosage forms. Processes, 1(2), 67–127.

[30] Ezike, T. C., Okpala, U. S., Onoja, U. L., Nwike, P. C., Ezeako, E. C., Okpara, J. O., Okoroafor, C. C., Eze, S. C., Kalu, O. L., Odoh, E. C., Nwadike, U., Ogbodo, J. O., Umeh, B. U., Ossai, E. C., & Nwanguma, B. C. (2023). Advances in drug delivery systems, challenges and future directions. Heliyon, 9(6), e17488.

[31] Patra, J. K., Das, G., Fraceto, L. F., Campos, E. V. R., Del Pilar Rodríguez-Torres, M., Acosta-Torres, L. S., Díaz-Torres, L., Grillo, R., Swamy, M. K., Sharma, S., Habtemariam, S., & Shin, H. S. (2018). Nano based drug delivery systems: recent developments and future prospects. Journal of Nanobiotechnology, 16(1), 1-33.

[32] Sun, C. C., & Davé, R. N. (2022). Crystal and particle engineering – an indispensable tool for developing and manufacturing quality pharmaceutical products. Pharmaceutical Research, 39(12), 3041–3045.

[33] Dirik, M. (2023). Machine learning-based lung cancer diagnosis. Turkish Journal of Engineering, 7(4), 322–330.

Chapter 3

EXAMINATION OF SPECTROSCOPIC ANALYSIS METHODS USED IN TRACE ELEMENT DETECTION

*Sema ÖZTÜRK YILDIRIM[1]**

1 Prof. Dr., Department of Physics, Faculty of Sciences, Erciyes University 38039 Kayseri TURKEY, ORCID ID: 0000-0001-5962-5337

*Corresponding Author: email: ozturk@erciyes.edu.tr

1. INTRODUCTION

Trace elements hold an extremely important place in the physiology of living organisms (Fukuda, Ebara, Yamada et al., 2004; Fraga, 2005; Kvirikadze, 1964; Goyer, 1997). Metals or metalloids found in amounts less than 50 dg per gramme of body tissue, and which make up less than 0.1% of body mass, are considered trace elements. For normal physiological functions, the presence of trace elements and trace metals at specific levels is essential. Essential heavy metals such as iron, copper, zinc, cobalt, magnesium, iodine, selenium, and manganese can also be classified as trace elements. Some metals, such as iron, copper, zinc, cobalt, magnesium, iodine, selenium, and manganese, are essential for human physiology (Crisponi, 2021). The deficiency or absence of essential metals has been linked to various diseases or syndromes in humans and plays a role in physiological functions (Jomova, Makova, Alomar, Alwasel, Nepovimova, Kuca, Rhodes & Valko, 2022). These elements are very important for providing the body's natural functions, as well as for growth, development, and protective properties.

Trace elements are determined by the National Committee for Clinical Laboratory Standards (Parsons & Barbosa, 2007) and are listed under three main headings. Essential elements include iron, zinc, copper, selenium, iodine, manganese, molybdenum, chromium, and cobalt; non-essential elements include aluminium, boron, silicon, vanadium, tin, lithium, and strontium; and potentially toxic elements include lead, mercury, cadmium, arsenic, beryllium, thallium, antimony, and nickel. Essential trace elements are elements that cannot be synthesised in the body, are absolutely necessary for normal physiological functions, and whose deficiency leads to specific biochemical abnormalities. Non-essential trace elements are elements that can be found in the body but have no known specific biological functions. Potential toxic elements, even at low concentrations, are metallic or metalloid elements that can harm human health (Tchounwou, Yedjou, Patlolla & Sutton, 2012).

Trace element analyses are performed using spectroscopic analysis methods. While there are numerous national and international studies examining the relationship between trace elements and heavy metals detected in qualitative and quantitative research and cancer development, there is no consistent standard among the results obtained. This study will provide important information on spectroscopic analysis methods used for the detection of trace elements.

2. SPECTROSCOPIC ANALYSIS METHODS USED IN THE DETERMINATION OF TRACE ELEMENTS

Among the main methods used in trace element analysis are Atomic Absorption Spectroscopy (AAS), Inductively Coupled Plasma-Mass Spectrometry (ICP-MS), Inductively Coupled Plasma-Optical Emission Spectrometry (ICP-OES), X-ray Fluorescence Spectroscopy (XRF), and Neutron Activation Analysis (NAA).

2.1. Inductively Coupled Plasma-Mass Spectrometry (ICP-MS)

ICP-MS is one of the most important techniques due to its low detection limit for elements, low error rate for accuracy and precision, and high selectivity. Since 1980, it has continued to develop and is one of today's most preferred devices.

This is a system where molecular bonds are broken and ionised, then the ions are directed to a mass filter, separated by their mass-to-charge ratio, and measured. Figure 1 shows the ICP-MS device. Plasma is typically produced at atmospheric pressure in an argon environment, sustained by a high-frequency (30 MHz) energy field of 1000-2000 W. The temperature in the plasma varies between 6 and 10×10^3 K, which is suitable for atomic excitation and ionisation of element types. The quartz torch consists of three concentric tubes into which different argon flows are introduced. When the samples are introduced into the plasma, they undergo desolvation, vaporisation, atomisation, and ionisation before entering the mass analyser. There are many methods for introducing solid, liquid, or gaseous samples into plasma. Conventional pneumatic nebulisation is the most common method for liquids. Ions exiting the ICP are typically introduced to the low-pressure mass spectrometry interface via sampling and skimmer cones made of nickel.

The ions are then focused onto the mass analyser using a series of ion lenses, and positively charged ions are then separated according to their mass-to-charge ratios. Ions are typically detected and amplified by an electron multiplier. The quadrupole ICP-MS has been the most commonly used mass analyser in quadrupole ICP-MS. To achieve higher resolutions and thus To reduce isobaric interferences, for example, the 75As+ with 40Ar 35Cl+ interference, double-focusing sector field mass analysers are used. Time-of-flight mass spectrometry (TOF) has great potential for speciation analysis. The introduction of samples to the ICP source at atmospheric pressure makes it possible to combine separation techniques with ICP-MS. High-resolution mass spectrometers reduce the appearance of isobaric overlap while shifting the relevant ion to a different m/z through chemical reactions (Montaser, 1998; Horlick 1986).

Inductively Coupled Plasma Mass Spectrometry is used for the sensitive and rapid analysis of trace elements and metals. Highly sensitive and multi-element analysis can be performed. It is widely used in fields such as toxicology, nutrition science, clinical chemistry, and environmental medicine (Thomas, 2013).

Figure 1. Inductively Coupled Plasma Mass Spectrometer (ICP-MS) System

ICP-MS has a sensitivity limit of parts per trillion (ppt) for many elements. This feature is particularly important for the ultra-trace analysis of toxic metals. The analysed sample allows for the simultaneous measurement of both high and low concentrations of elements. It can quickly analyse approximately 75% of the elements in the periodic table. Additionally, ICP-MS, which can distinguish between different isotopes of elements, is important in metabolic studies, environmental monitoring, and nuclear medicine applications due to this feature. Analyses can typically be performed with very small sample volumes (typically 1-2 mL) (Nelms SM., 2005; Becker, 2013; Ivanenko et al., 2011). The biggest disadvantage of the method is that in complex biological matrices, the mass-to-charge ratios of some elements or molecular ions can overlap, leading to spectral interference or measurement errors. High-purity argon gas and other consumables are required for the system to function properly. The cost of ICP-MS instruments is quite high and their use requires technical knowledge and maintenance (Agatemor & Beauchemin, 2011; Ammann, 2007; Szpunar, 2000). ICP-MS is widely used in the analysis of biological samples (Cihan & Öztürk Yıldırım, 2011; Cihan, Öztürk Yıldırım, Sofikerim & Göcen, 2013; Cihan, Sözen & Öztürk Yıldırım, 2011; Öztürk Yıldırım & Cihan, 2010; Laborda et al., 2016; Uslu et al., 2025).

2.2. Inductively Coupled Plasma-Optical Emission Spectrometry (ICP-OES)

The basic principle of inductively coupled plasma-optical emission spectrometry (ICP-OES) relies on the spontaneous emission of photons produced from ions or atoms, and the excitation of these ions and atoms by a radio frequency discharge (Majumdar & Dubey, 2017). Figure 2 shows the ICP-OES device. In ICP-OES, samples are introduced into an inductively coupled argon plasma through a sample injection system where molecules are atomised and ionised in the plasma and finally excited (Soltanpour, Johnson, Workman, Jones, & Miller, 1996). When electrons return from an excited energy level to a lower energy level, ions and atoms release photons, which are called ionic or atomic emission, and the emission is then collected on a detector using Echelle or Rowland circle optics, which separate the different emission wavelengths from each (Ghosh et al., 2013). The detector then measures the emission signal intensities of the relevant wavelengths, which correspond to the energy difference between the excited and ground states of the electron, and the strength of the emission signal is proportional to the element's abundance in the plasma (Bibinov, Halfmann, Awakowicz, & Wiesemann, 2007). In ICP-OES, a sample, typically a liquid sample, is injected into the central channel of a radiofrequency (RF)-induced argon plasma; here, the liquid sample is converted into an aerosol form through a process called aerosol nebulisation (Donati, Amais, & Williams, 2017). ICP-OES, which maintains very high temperatures (8000–10000K) to rapidly dry and vaporise the aerosol, releases the elements as free atoms in the gaseous state as an analyte (Warren, 1993).

Additionally, the aerosol sample is transported to the plasma, where it is dissolved, vaporised, atomised, and ionised with the help of the plasma sample, converting it into ions that are then excited to a higher energy state by emitting photons, after which the ground state is reached (Walkup, Saenger, & Selwyn, 1986). Subsequently, photons from the ICP OES are collected with the aid of a concave mirror or lens, and this focussing optical lens, along with a wavelength selection device called a monochromator and the selected specific wavelength, forms an image of the inductively coupled plasma (ICP) at the entrance aperture. It is then converted by a detector consisting of a photodetector, which converts them into an electrical signal, which is then processed, amplified, and recorded by a computer. A monochromator is a simple monochromator or a photomultiplier tube (PMT) that can be used for single-element detection, while a combination of a polychromator and an advanced array detector is used for simultaneous multi-element detection (up to 70 elements) (Thompson, 2012).

Inductively Coupled Plasma-Optical Emission Spectrometry (ICP-OES) is a powerful spectroscopic analysis technique used for the sensitive and rapid analysis of trace elements and metals. Developed in the late 1960s, this technique began to be studied and used in medical and biological research. With its high sensitivity, wide linear working range, and ability to analyse multiple elements, it is frequently used in fields such as toxicology, clinical biochemistry, pharmacology, etc. (Hou & Jones, 2000).

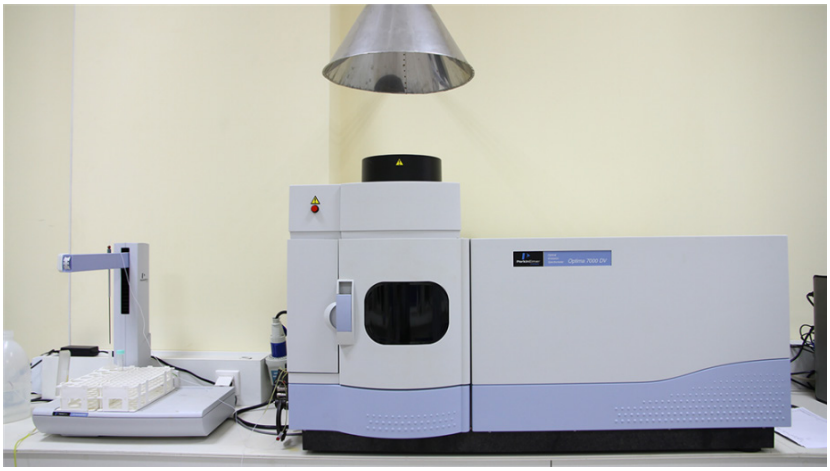

Figure 2. Inductively Coupled Plasma/Optical Emission Spectrometer System

ICP-OES has detection limits at the parts per billion (ppb) level for many elements. It can quickly analyse most of the elements in the periodic table (Barnard, 1993; Boss & Fredeen, 1997). Another significant advantage of ICP-OES is that it is less susceptible to matrix effects compared to ICP-MS. High-temperature plasma effectively atomises and ionises most matrix components, which reduces matrix-induced interferences. Additionally, the operating costs of ICP-OES are generally lower than those of ICP-MS. The device is easier to use and maintain (Cornelis et al., 2005).

2.3. X-ray Fluorescence Spectroscopy (XRF)

The XRF spectroscopy technique is based on the principle of interaction between the sample being analysed and the X-ray beam obtained from a radioactive source. In this technique, the elements to be determined are excited by absorbing the primary beam incident on the sample, and then they emit their characteristic fluorescent X-rays. Therefore, in the XRF spectroscopy technique, semi-quantitative and quantitative determinations of elements with atomic numbers greater than oxygen can be achieved through X-ray emission spectra obtained by placing the sample within the target area of an X-ray tube (Beşergil, 2020).

XRF spectrometers can generally be divided into two main categories, depending on the detector system: wavelength dispersive XRF (WDXRF) and energy dispersive XRF (EDXRF) spectrometers. As shown in Figure 3, WDXRF uses a wavelength diffraction system to separate the characteristic wavelengths emitted by the sample. The X-ray source irradiates the sample, and a portion of the characteristic fluorescence radiation from the sample is directed to the surface of the diffraction system through a collimator. According to Bragg's law, individual wavelengths are directed to a second collimator and delivered to the detector. An angle meter is used to maintain the necessary angle between the diffraction system and the detector. Thanks to the high-resolution power of crystals and multilayer structures, photons corresponding to characteristic lines with similar energies can be detected without interacting with each other, thus providing high selectivity in the analysis (Marguí et al., 2014). In the EDXRF technique, which has a relatively simpler structure, the X-ray is irradiated onto the sample to be analysed at a 45° angle. The total reflection XRF (TXRF) technique is actually based on the EDXRF technique. The main difference between EDXRF and TXRF is the angle at which the X-ray enters the sample. In the TXRF technique, the X-ray is irradiated at a grazing angle of a few milliradians. Since the direction of the X-ray is almost parallel to the surface of the sample, the X-ray is completely reflected. Thus, absorption of the beam by the substrate on which it is placed is prevented, scattering and background noise are significantly reduced, and the detection limit can be improved (ACTTR Inc., 2020).

X-ray fluorescence (XRF) spectroscopy is an analytical technique used to determine the elemental composition of materials. This method is based on measuring the characteristic fluorescent X-rays that result from the interaction of X-rays with matter. XRF spectroscopy has applications in various fields and is frequently used, especially in metallurgy, environmental science, and medical research (Jenkins, 1999).

Figure 3. X-ray Fluorescence Spectrometer System

One of the most significant advantages of XRF spectroscopy is that it is a non-destructive analytical method. Sample preparation is generally minimal, and the sample is not damaged during analysis. Measurements are quite fast; they can usually be completed in a few seconds to a few minutes. XRF has the ability to measure over a wide range, from 100% down to ppm levels. It can be used for analysing samples in solid, liquid, and powder form (Beckhoff, Kanngießer, Langhoff, Wedell & Wolff, 2006; Brouwer, 2010). The detection of light elements (usually lighter than sodium) is difficult and may require special equipment. Additionally, the surface composition of the sample being different from the bulk composition can lead to misleading results. Matrix effects, especially in complex samples, can affect measurement accuracy. Therefore, appropriate calibration standards and matrix correction methods must be used for accurate results. XRF spectroscopy does not provide information about chemical bonding; it only gives information about elemental composition. XRF spectroscopy is frequently used in a wide variety of fields (Rousseau, 2006; Ancharov, Potts & Nalini, 2008).

2.4. Atomic Absorption Spectroscopy (AAS)

Atomic absorption spectrometry (AAS) is a method based on measuring the absorption of light by atoms formed in the gas phase. AAS is used for the quantitative determination of approximately 70 metals and metalloids. Basically, AAS is not suitable for the direct determination of non-metals (halogens, sulphur, nitrogen, etc.) because they absorb in the far (vacuum) UV range where air components (nitrogen, oxygen) also absorb. An atomic absorption spectrometer consists of 4 basic components: an emission source, an atomiser, a wavelength selector, and a detector.

Generally, AAS is dedicated to solution analysis. Therefore, solid samples are digested prior to analysis using mineral acids, and oxidants with and without heating.

For the atomisation of the analyte using thermal energy, the sample solution is aspirated into a flame or injected into a graphite tube as 10 to 50 µL, which is approximately 4-5 cm long, 1 cm in diameter, and heated according to a pre-adjusted time-temperature program up to 3000 °C.

Electrons of the atomised analyte are promoted to higher orbitals for a short period of time by the radiation energy emitted from an appropriate light source. The amount of energy required to promote electrons to higher orbitals should be equal to the difference between the energies of the excited and ground state levels, which is specific to each element. The absorbance, which is the logarithm of the ratio of source intensities before and after absorption, is measured by the detector and related to analyte concentration using Lambert-Beer's Law.

Atomic Absorption Spectroscopy (AAS) has become a routine method for determining the quantitative amounts of many metals and metalloids. Atomic absorption spectroscopy is a powerful analytical technique widely used in the qualitative and quantitative analysis of trace elements and metals. Developed in 1955 by Australian physicist Alan Walsh, this technique has since become an indispensable tool in analytical chemistry. The principle behind AAS is that atoms found in their free state in elements absorb light at their specific wavelengths. Figure 4 shows the Atomic Absorption Spectrophotometer (AAS) System.

The working principle is that the electrons of an atom can transition between these levels while residing at specific energy levels. When an electron in its ground state absorbs light of a specific wavelength, it transitions to a higher energy level. This amount of absorption is directly proportional to the concentration of the element in the sample, which is explained by Beer-Lambert's law (Skoog, West, Holler & Crouch, 2013). This relationship forms the basis for the use of AAS in quantitative analyses. The basic components of an AAS system are the light source, atomisation system, monochromator, detector, and signal processing unit. A hollow cathode lamp is generally used as the light source. This lamp contains a cathode made of the pure metal or alloy of the element to be analysed and produces an element-specific emission spectrum (Butcher & Sneddon, 1998). The atomisation system is used to convert the sample into atomic vapour, and there are two types: the flame atomiser and the electrothermal atomiser (graphite furnace).

While a flame atomiser is used in Flame Atomic Absorption Spectrometry systems, an electrothermal atomiser is used in Graphite Furnace Atomic Absorption Spectrometry systems (Tsalev & Zaprianov, 1999).

Figure 4. Atomic Absorption Spectrophotometer (AAS) System

In Flame Atomic Absorption Spectrometry, a liquid sample is converted into a fine aerosol with the aid of a nebuliser and sprayed into the flame. The flame is usually composed of an air-acetylene or nitrous oxide-acetylene mixture, and its temperature ranges from 2100-2800°C. This temperature causes the compounds in the sample to decompose into their constituent atoms. In Graphite Furnace Atomic Absorption Spectrometry, the sample is placed inside a small tube made of graphite and heated with an electric current. The temperature is gradually increased through the drying (100-120°C), then ashing (400-800°C), and finally atomisation (2000-2800°C) stages. With these stages, GFAAS provides higher sensitivity compared to FAAS, allowing for analysis with smaller sample volumes (typically 10-20 µL) (Welz, Vale, Borges & Heitmann, 2007). A monochromator separates the beam of light from the light source, allowing only the wavelength of interest to reach the detector. The detector is typically a photomultiplier tube that converts incoming light into an electrical signal. Finally, the signal processing unit converts this electrical signal into concentration information (Hou & Jones, 2000; World Health Organisation, 2019).

The application area of AAS in medical and biomedical research is quite extensive. In the field of toxicology, AAS is widely used in the diagnosis and monitoring of heavy metal poisoning.

2.5. Neutron Activation Analysis (NAA)

Neutron Activation Analysis (NAA) is an elemental analysis method. In this method, the sample is bombarded with neutrons, and the resulting radiation from the interaction of the sample's constituent elements' isotopes with neutrons is measured to perform a qualitative and quantitative analysis of the sample. Qualitative analysis is performed by utilising the type of radiation emitted by the resulting radioisotopes, i.e., their α, β, γ energies, and half-lives. Quantitative analysis, on the other hand, involves determining the amount of the radioisotope formed in the sample by measuring its radioactivity. The theory behind the neutron activation analysis method is as follows: if a uniform and stable neutron flux is applied to the material being analysed for a specific period, some of the stable isotopes of the elements contained in the material will absorb a neutron and form a new, and often excited, isotope.

The nuclei in this state:

1) Transition to a stable state by emitting characteristic gamma photons at various energies for around 10-12 seconds. However, these gamma rays are immeasurable because they are very short-lived.

2) Stable isotopes can be formed. In this case, gamma radiation and measurement are not relevant.

3) The resulting isotope emits gamma rays to reach a stable state after α or β decay with a detectable half-life, transforming into a new element.

These rays have a characteristic energy value that identifies the isotope. By determining the energies of these gamma rays, the presence of the elements that make them up can be qualitatively identified. Or their intensity can be measured to determine their quantity. In irradiated samples, one isotope is formed on one hand while decaying on the other. Saturation activity is reached when the rate of formation equals the rate of decay. It is assumed that saturation activity is reached approximately 10 half-lives after irradiation begins, and that the activity drops to zero approximately 10 half-lives after irradiation ends.

Neutron activation analysis (NAA) is a nuclear technique used to determine elemental and isotopic composition. This method relies on the production of radioactive isotopes of elements in samples bombarded with neutrons, followed by the measurement of the characteristic gamma rays emitted by these isotopes. NAA has various applications in environmental science, archaeology, forensic science, and materials science. The basic working principle of the technique begins with the sample being

subjected to neutron bombardment, typically in a nuclear reactor or neutron generator.

Neutrons are captured by the nuclei of atoms in the sample, leading to the formation of unstable radioisotopes. These radioisotopes decay with characteristic half-lives and emit gamma rays at specific energies. Emitted gamma rays are measured with special detectors such as high-purity germanium detectors, and the resulting gamma spectrum is analysed to determine the elemental composition of the sample (Glascock & Neff, 2003; Alfassi, 1990).

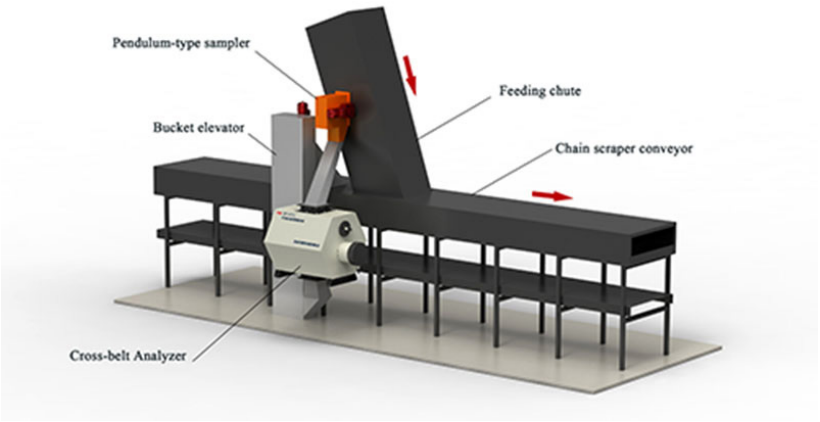

Figure 5. Neutron Activation Analysis System

One of the most important features of NAA is its ability to detect many elements at ppb (parts per billion) or lower levels. This high sensitivity makes the technique particularly valuable in trace element analysis. Additionally, with NAA, a single measurement can simultaneously analyse up to 30-40 elements. This multi-elemental analysis capability allows for the rapid and comprehensive characterisation of complex samples. Another important feature of NAA is matrix independence; the analysis results are generally not affected by the chemical form of the sample. This allows samples from different matrices to be analysed with comparable results.

Additionally, NAA has the ability to determine the concentrations of specific isotopes, making it ideal for studies requiring isotopic analysis (Greenberg, 2011). Among the advantages of NAA are its high sensitivity and accuracy, minimal sample preparation requirements, non-destructive analysis capability, and wide dynamic range. Thanks to high sensitivity and accuracy, precise and accurate measurements can be made for many elements even at very low concentrations. Minimal sample prepa-

ration reduces the risk of contamination, while non-destructive analysis capability ensures the sample is preserved even after analysis. This feature is particularly valuable in the analysis of archaeological and artistic artefacts. NAA's wide dynamic range allows for the analysis of both major and trace elements in the same sample.

NAA also has some disadvantages. It's quite expensive. The installation and operating costs are quite high due to the need for a nuclear reactor or neutron generator. Additionally, post-analysis samples can be radioactive, requiring special waste management.

For some elements, the analysis time can take days or weeks, which may not be suitable for situations requiring quick results. NAA is not suitable for some light elements (H, He, Li, Be) and some heavy elements, which limits the elemental coverage of the technique. In biomedical research, it is used to study the role of trace elements in biological systems. In materials science, it is used as an important tool for characterising high-purity materials. Neutron activation analysis is a powerful and versatile technique for elemental and isotopic analysis. Its advantages, such as high sensitivity, multi-element analysis capability, and matrix independence, make it valuable in many scientific and industrial applications.

4. CONCLUSION

Inductively Coupled Plasma-Mass Spectrometry (ICP-MS) ranks first as the most sensitive method in trace element analysis. Inductively Coupled Plasma-Optical Emission Spectrometry is a moderately preferred method in applications requiring multi-element analysis. X-ray fluorescence spectroscopy is a fast and non-destructive analysis method and is quite useful. Neutron Activation Analysis is preferred for use in special research projects requiring high sensitivity and is a rather expensive technique. Atomic Absorption Spectroscopy is the most commonly used technique in clinical laboratories. It is very widely preferred due to its ease of use and low cost. When determining the analytical method to be chosen for detecting the elements in the work, many factors should be considered in making the decision. Before performing trace element analysis, the spectroscopic analysis method should be determined by considering parameters such as which element requires what level of sensitivity, sample quantity, sample preparation, speed of spectroscopic analysis, cost, and multi-element analysis. Using the aforementioned spectroscopic analysis methods, trace elements can be analysed and comparisons can be made between the methods. Spectroscopic analysis methods used for measuring trace elements constitute a wide range, each offering its own unique advantages and disadvantages.

REFERENCES

ACTTR Inc. (2020). Introduction to TXRF.

Agatemor C, Beauchemin D. (2011). Matrix effects in inductively coupled plasma mass spectrometry: A review. Anal Chim Acta. 706(1):66-83.

Alfassi, Z. B. (Ed.). (1990). Activation analysis (Vol. 1). CRC press.

Ammann, AA. (2007). Inductively coupled plasma mass spectrometry (ICP MS): a versatile tool. J Mass Spectrom. 42(4):419-427.

Ancharov, A. I., Potts, P. J., & Nalini, H. (2008). Micro-X-ray fluorescence analysis in geochemistry and archaeology. X-Ray Spectrometry, 37(4), 363-371.

Barnard, T. W., Crockett, M. I., Ivaldi, J. C., et al. (1993). Solid-state detector for ICP-OES. Analytical Chemistry 65 1231–1239.

Beşergil, B. (2020). Enstrümantal Analiz Temel İlkeler,

Beckhoff, B., Kanngießer, B., Langhoff, N., Wedell, R., & Wolff, H. (2006). Handbook of Practical X-Ray Fluorescence Analysis. Springer.

Becker, JS.(2013). Imaging of metals in biological tissue by laser ablation inductively coupled plasma mass spectrometry (LA-ICP-MS): state of the art and future developments. J Mass Spectrom. 48(2):255-268.

Bibinov, N., Halfmann, H., Awakowicz, P., & Wiesemann, K. (2007). Relative and absolute intensity calibrations of a modern broadband echelle spectrometer. Measurement Science and Technology, 18(5), 1327.

Boss, CB, Fredeen & KJ. Concepts (1997)., Instrumentation and Techniques in Inductively Coupled Plasma Optical Emission Spectrometry. Perkin Elmer.

Brouwer, P. (2010). Theory of XRF: Getting acquainted with the principles. PANalytical BV.

Butcher, DJ & Sneddon, J. A. (1998). Practical Guide to Graphite Furnace Atomic Absorption Spectrometry. John Wiley & Sons.

Cihan, YB & Öztürk Yıldırım, S. (2011). Biological Trace Element Research, A Discriminant Analysis of Trace Elements in Scalp Hair of Healthy Controls and Stage-IIIB Non-small Cell Lung Cancer (NSCLC) Patients, 144(1-3):272-94.

Cihan, YB, Öztürk Yıldırım, S. Sofikerim, MM & Göcen, EE. (2013). Turkish Journal of Geriatrics. Comparison of trace element levels between aged T1 stage bladder cancer patients and normal donors using the ICP/MS method, 16(1).

Cihan, YB, Sözen, S. & Öztürk Yıldırım, S. (2011). Biological Trace Element Research. Trace Elements and Heavy Metals in Hair of Stage III Breast Cancer Patients, 144(1-3):360-79.

Cornelis R, et al. (2005). Handbook of Elemental Speciation II: Species in the Environment, Food, Medicine and Occupational Health. John Wiley & Sons.

Crisponi G. (2021). Essential and Toxic Metal Ions in Human Health and Disease;

From Chemical Features to Clinical Roles. Current medicinal chemistry, 28(35), 7187–7189.

Donati, G. L., Amais, R. S., & Williams, C. B. (2017). Recent advances in inductively coupled plasma optical emission spectrometry. Journal of Analytical Atomic Spectrometry, 32(7), 1283-1296.

Fukuda, H., Ebara, M., Yamada, H., et al. (2004). Trace elements and cancer. J Jpn Med Assoc, 47:391–5.

Fraga, CG. R(2005). Relevance, essentiality and toxicity of trace elements in human health. Mol Aspects Med., 26:235–44.

Glascock, M. D., & Neff, H. (2003). Neutron activation analysis and provenance research in archaeology. Measurement Science and Technology, 14(9), 1516.

Ghosh, S., Prasanna, V. L., Sowjanya, B., Srivani, P., Alagaraja, M., & Banji, D. (2013). Inductively coupled plasma–optical emission spectroscopy: a review. Asian Journal of Pharmaceutical Analysis, 3(1), 24-33.

Goyer, RA. (1997). Toxic and essential metal interactions. Annu Rev Nutr.17:37-50. (PMID:9240918).

Greenberg, R. R., Bode, P., & De Nadai Fernandes, E. A. (2011). Neutron activation analysis: a primary method of measurement. Spectrochimica Acta Part B: Atomic Spectroscopy, 66(3-4), 193-241.

Horlick, G., & Tan, S. H. (1986). Background spectral features in inductively coupled plasma/mass spectrometry. Applied Spectroscopy, 40(4), 445-460.

Hou, X. & Jones, BT. (2000). Inductively coupled plasma/optical emission spectrometry. In: Encyclopedia of Analytical Chemistry. John Wiley & Sons.

Ivanenko, NB, et al. (2011). Determination of trace elements in biological fluids. J Anal Chem. 66(9):784-799.

Jenkins, R. (1999). X-ray Fluorescence Spectrometry. Wiley.

Jomova, K., Makova, M., Alomar, S. Y., Alwasel, S. H., Nepovimova, E., Kuca, K., Rhodes, C. J., & Valko, M. (2022). Essential metals in health and disease. Chemicobiological interactions, 367, 110173. https://doi.org/10.1016/j.cbi.2022.110173

Kvirikadze, NA. (1964). Chemical form of Mn, Pb, Cu, Ag, Zn, Ti, and Ni in malignant tumors of urinary bladder. Soobshcheniya Akad Nauk Gruzinskoi SSR. 35:579–86.

Laborda, F., et al. (2016). Detection, characterization and quantification of inorganic engineered nanomaterials: A review of techniques and methodological approaches for the analysis of complex samples. Anal Chim Acta. 904:10-32.

Majumdar, A. J., & Dubey, N. (2017). Applications of inductively coupled plasma-atomic emission spectrometry (ICP-OES) in impurity profiling of Pharmaceuticals. International Journal of Pharmacy & Life Sciences, 8(1), 5420-5425.

Marguí, E., Zawisza, B. & Sitko, R. (2014). Trace and ultratrace analysis of liquid samples by X-ray fluorescence spectrometry. Içinde TrAC - Trends in Analytical Chemistry (C. 53, ss. 73–83). Elsevier B.V.

Montaser, A. & Golightly, DW.(1992). Inductively Coupled Plasmas in Analytical Atomic Spectrometry. 2nd ed. Wiley-VCH.

Montaser, A. (1998). Inductively Coupled Plasma Mass Spectrometry, New YORK, A.B.D.: John Wiley & Sons Publishing.

Nelms, SM. (2005). Inductively Coupled Plasma Mass Spectrometry Handbook. Blackwell Publishing.

Öztürk Yıldırım, S. & Cihan YB. Azerbaijan Journal of Physics Fizika (2010). Application Of Inductively Coupled Plasma Mass Spectrometry (ICP/MS) To Detectıon Of Trace Elements, Heavy Metals And Radıoısotopes In Scalp Hair.

Parsons P. J.& Barbosa F. J.(2007). Atomic spectrometry and trends in clinical laboratory medicine, Spectrochimica Acta. 62(9), 992–1003.

Rousseau, R. M. (2006). Corrections for matrix effects in X-ray fluorescence analysis—A tutorial. Spectrochimica Acta Part B: Atomic Spectroscopy, 61(7), 759-777.

Skoog, DA., West, DM., Holler, FJ. & Crouch SR. (2013). Fundamentals of Analytical Chemistry. 9th ed. Cengage Learning.

Soltanpour, P. N., Johnson, G. W., Workman, S. M., Jones Jr, J. B., & Miller, R. O. (1996). Inductively coupled plasma emission spectrometry and inductively coupled plasma-mass spectrometry. Methods of Soil Analysis: Part 3 Chemical Methods, 5, 91-139.

Szpunar, J. (2000). Bio-inorganic speciation analysis by hyphenated techniques. Analyst. 125(5):963-988.

Thomas, R. (2013). Practical Guide to ICP-MS: A Tutorial for Beginners. 3rd ed. CRC Press.

Thompson, M. (2012). Handbook of inductively coupled plasma spectrometry. Berlin, Almanya: Springer International Publishing.

Tsalev, DL. & Zaprianov, ZK. (1999).Atomic Absorption Spectrometry in Occupational and Environmental Health Practice. 2nd ed. CRC Press.

Uslu, E., Alabaz, Ö., Eray, İ.C., Topal, U., Aydın, İ, Yavuz B., Açıkalın A., Aydınoğlu S. & Marinelli A.Y. (2025). 8. Çukurova Gastro-İntestinal Hastalıklar ve Cerrahisi Kongresi, Sağlıklı ve kanserli dokularda mikro dalga yakma yöntemiyle hazırlanan örneklerdeki element miktarlarının indüktif olarak eşleştirilmiş plazma- kütle spektrometresi(Icp-ms) yöntemiyle belirlenerek kıyaslanması, S24, 24-26 Nisan 2025, Anemon Otel, Adana.

Welz, B., Vale, MG., Borges, DL. & Heitmann U. (2007). Progress in direct solid sampling analysis using line source and high-resolution continuum source electrothermal atomic absorption spectrometry. Anal Bioanal Chem. Dec;389(7-8):2085-95.

World Health Organization. Lead poisoning and health. Published 2019.

Warren, T. (1993). Development of an atomic fluorescence spectrometer for the hydride-forming elements. Journal of Analytical Atomic Spectrometry, 8(1), 71-77.

Walkup, R. E., Saenger, K. L., & Selwyn, G. S. (1986). Studies of atomic oxygen in O2+ CF4 rf discharges by two-photon laser-induced fluorescence and optical emission spectroscopy. The Journal of Chemical Physics, 84(5), 2668-2674.

Chapter 4

CRYSTAL STRUCTURE OF $C_{13}H_{12}N_2OS$, HIRSHFELD SURFACE ANALYSIS, MOLECULAR ELECTROSTATIC POTENTIAL (MEP) ANALYSIS AND FRONTIER MOLECULAR ORBITAL ANALYSIS

Sema ÖZTÜRK YILDIRIM[1]*

Hakan BÜLBÜL[2]

1 Prof. Dr., Department of Physics, Faculty of Sciences, Erciyes University 38039 Kayseri TURKEY, ORCID ID: 0000-0001-5962-5337

*Corresponding Author: email: ozturk@erciyes.edu.tr

2 Lect. PhD, Department of Physics, Faculty of Arts & Sciences, Ondokuz Mayis University, 55139 Samsun, Türkiye, ORCID ID: 0000-0002-8586-5075

1. INTRODUCTION

The structure of the $C_{13}H_{12}N_2OS$ (S-2-aminophenyl N-phenylcarbamothioate) compound a new product of our ongoing work, was determined using single-crystal X-ray diffraction technique (Yıldırım Öztürk, S. et al., 2018; Doğan,Ş.D. et al., 2020; Yıldırım Öztürk, S. et al., 2018). As part of our studies in this area was obtained from the condensation reaction of 2-aminobenzenethiol with isocyanatobenzene and published (Öztürk Yıldırım & Butcher, 2018). Organic carbamothioates are a class of compounds that play an important role in the synthesis of pharmaceuticals and agricultural chemicals (Torrico-Vallejos et al., 2011; Belkhir et al., 2015). The S-2-aminophenyl N-phenylcarbamothioate (Fig. 1) was obtained from the condensation reaction of 2-aminobenzenethiol with isocyanatobenzene. The data collection conditions and parameters of refinement process are listed in Table 1. In the title compound the benzene rings are inclined to one another by 83.5 (1)º and a short intramolecular C—H. . .O contact is observed. In the crystal, molecules are linked by N—H. . .O and N—H. . . N hydrogen bonds, generating (001) sheets (Table 2). The evaluation of the electrostatic, dispersion and total energy frameworks indicates that the stabiliation is dominated by the dispersion energy contribution. Moreover, the molecular structure optimized by density functional theory(DFT) at the B3LYP/6-311G(d,p) levelis compared with the experimentally determined molecular structure in the solidstate. The HOMO–LUMO behaviour was elucidated to determine the energygap.

Table 1. *Crystal data and structure refinement parameters.*

Chemical formula	$C_{13}H_{12}N_2OS$
Color/shape	Plate, clear light colourless
Formula weight	244.31
Temperature	100 K
Crystal system	Orthorhombic
Space group	*Pbca*
Unit cell parameters	a = 9.4505 (6) Å b = 10.4021 (8) Å c = 24.3308 (18) Å
Volume	2391.8 (3) $Å^3$
Z	8
Density	1.357 Mg m^{-3}

Absorption correction	Gaussian (CrysAlis PRO; Rigaku OD, 2015)
Tmin, Tmax	0.712, 1.000
No. of measured, independent and observed [I > 2_(I)] reflections	37562, 5122, 2960
R[F2 > 2_(F2)], wR(F2), S	0.094, 0.217, 1.08
No. of reflections	5122
No. of parameters	166
H-atom treatment	H atoms treated by a mixture of independent and constrained refinement
$\Delta\rho_{max}$, $\Delta\rho_{min}$ (e Å^{-3})	0.89, -0.49

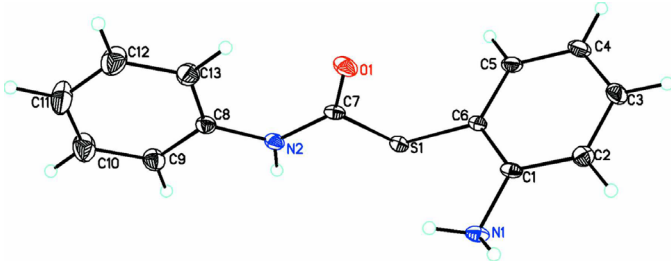

Figure 1. *The molecular structure of the title compound, with atom labelling. Displacement ellipsoids are drawn at the 50% probability level*

Table 2. Hydrogen bonding geometry for the titled compound.

D—H···A	D—H	H···A	D···A	D—H···A
N1—H1N1···O1^{i}	0.85 (4)	2.18 (4)	2.899 (3)	141 (4)
N1—H1N2···S1^{ii}	0.89 (4)	2.93 (3)	3.340 (3)	110 (3)
N2—H2N···N1^{ii}	0.85 (4)	2.17 (4)	2.993 (4)	164 (4)
C5—H5A···S1^{iii}	0.95	3.00	3.782 (3)	141
C13—H13A···O1	0.95	2.32	2.926 (4)	121

Symmetry codes: (*i*) x+1/2, −y+3/2, −z+1; (*ii*) −x+2, −y+1, −z+1; (*iii*) −x+1, −y+1, −z+1.

2. MOLECULAR THEORETICAL CALCULATIONS

When energy calculations for molecules cannot be done directly using the Schrödinger equation, approximate calculation methods called molecular dynamics calculations are used.

2. 1. Ab-initio molecular orbital methods

Ab initio molecular orbital methods refer to a set of computational techniques based on the principles of quantum mechanics for calculating the electronic structures and properties of molecular systems. The term "ab initio" is Latin for "from the beginning" or "from first principles," and these methods are used to calculate the electronic structures and properties of molecular systems without relying on experimental data. Actually, the Ab initio method is a quantum mechanical approach used to calculate the structures and properties of molecules. This method does not rely on molecular mechanics or experimental data; instead, the behaviour of molecules is predicted using fundamental physical constants and approximate solutions to the Schrödinger equation. This approach allows for the examination of molecular systems at the atomic level and enables the theoretical calculation of many properties such as chemical bonds, molecular structures, reaction mechanisms, and spectral properties (Jensen, 1999). In ab initio calculations, two different mathematical approaches are used: Hartree-Fock (HF) and Density Functional Theory (DFT). The Hartree-Fock (HF) model defines an explicit expression for the energy as a function of the molecular wave function ψ. This model does not consider correlation effects and uses an average potential for electron-electron interactions. The HF method is used particularly in areas such as calculating molecular frequencies and determining molecular geometry. However, because it doesn't fully account for correlation effects in real systems, it may provide limited accuracy in some cases. In the DFT (Density Functional Theory) model, the explicit expression for energy depends on the electron density ρ instead of the molecular wave functions ψ. DFT is a method that provides much more accurate results in determining molecular properties (such as electron distribution, reactivity, and polarisability). This method models the electronic structure and chemical bonds more precisely based on the density of electrons. While

the HF model is simpler and may be sufficient for some applications, the DFT model is more comprehensive and provides more accurate results, making it preferable, especially when studying molecular properties.

2.2. Density functional theory (DFT)

DFT (Density Functional Theory) was initially used only to find the ground state energy of a single molecule. However, it is a method developed by Kohn and Sham and has a similar structure to the Hartree-Fock method (Kohn & Sham, 1965). In the DFT method developed by Kohn and Sham, the electron density is expressed as a linear combination of basis functions similar in mathematical form to the HF (Hartree-Fock) orbitals. However, the exchange-correlation potential term in the Kohn-Sham equations of DFT is not simply a function of electron density, as it is in HF. The term "potential exchange correlation" has been used more generally. This exchange correlation potential is expressed as a function of electron density and allows for the solution of the Schrödinger equation. Using electron density allows for the integrals that need to be solved for the Coulomb interaction to be solved only over the electron density, and for the calculations to include some electron correlations (Chermette, 1998; Young, 2001). Methods such as the local density approximation and density functional theory generally handle correlation in a simpler manner. DFT can combine the local density approximation and density functional theory to more accurately calculate the effect of correlation. This is applied as a correlation term added to the Hartree-Fock energy.

2.3. Hartree-Fock theory

This approach, formulated by Hartree, is based on the time-independent particle model. In this model, each electron moves within an effective potential that accounts for the average effect of the nucleus's attractive field and the repulsive interactions with other electrons. Electrons, moving under this effective potential, try to minimise the system's energy. In a multi-electron system, each electron is expected to be defined by its own wave function. In the Hartree-Fock approximation, the motion of each electron occurs under an effective potential that interacts with the presence of other electrons. Hartree's

proposal is that these equations can be solved by an iterative method called the "self-consistent field." So, the calculation of electron interactions and the recalculation of the effective potential are repeated in a loop to more accurately predict the electronic structure. This method forms the basis of the Hartree-Fock method and is an important tool in the calculation of molecular structures (Becke, 1993).

2.4. B3LYP hybrid density functional theory

HF theory does not provide good results for exchange energy and cannot calculate correlation energies. However, it provides a suitable expression for kinetic energy. DFT calculates the exchange and correlation energies of molecules more accurately. Therefore, for a complete energy accounting of a system, hybrid models have been developed that combine the energy expressions of these two theories, rather than using only HF or only DFT. These hybrid models can better calculate many properties for molecules, such as total energy, bond lengths, and ionisation energies. In this way, more accurate results are obtained than with pure HF or DFT models. While HF theory provides suitable expressions for kinetic energy, DFT can better model exchange and correlation energies. Hybrid models, by combining these advantages, provide more accurate results for important quantities such as bond lengths and ionisation energies in the total energy calculation of molecules.

2.5. Gaussian09 and GaussView6

The Gaussian09 program is a software package used to perform many electronic structure modelling calculations and quantum chemical calculations. This program can perform various calculations using Ab initio, semi-empirical, and molecular mechanics methods. Density functional theory (DFT), Hartree-Fock theory (HF), and other advanced quantum chemistry methods are used to calculate the electronic structures, energy levels, optical and spectral properties, reaction energies, transition states, and much more of molecules. Gaussian09 is a critical tool for research in fields such as chemistry, biochemistry, and materials science. Some calculations that can be done with this program include: Ideal geometric optimisations of atoms and molecules can be performed. This allows for the determination of the most stable and energetically lowest configurations

of molecular structures. The vibrational frequencies of atoms can be calculated based on their energies. This is used to study the vibrational behaviour of molecular systems. Properties such as HOMO, LUMO, and band gap can be calculated. Simulations can be performed for spectral properties such as UV-Vis, IR, and NMR, allowing for comparison with experimental spectra. The energies possessed by atoms and molecules can be calculated. This helps determine the energy profiles of molecular systems. The force constants and dipole moments of atoms and molecules can be calculated. This is important for understanding the mechanical and electrical properties of molecular systems. Transition states and activation energies in chemical reactions can be determined, allowing for the study of reaction mechanisms. Solvation models such as the polarisable continuum model (PCM) are available to model the behaviour of molecules in water or other solvents. Additionally, the stability of the molecular wave function can be examined using the Gaussian09 program. By navigating potential energy levels, transition states and possible reaction pathways can be determined. These calculations can be performed for molecules in various environments, such as crystalline, solution, or gaseous states (Frisch et al., 2009). “GaussView6” is a molecular modelling software used within the Gaussian software package for creating, displaying, analysing, and visualising molecular structures. This software can read output files from Gaussian calculations and present this data in a user-friendly interface for visual inspection of molecular structures.

2.6. Basis Set

The term “basis set” refers to the mathematical representations of atomic orbitals used in quantum chemical calculations to accurately represent the chemical properties of a system. In this context, basis sets typically consist of a group of functions optimised as contracted Gaussian functions (Dorsett & White, 2000). Basis sets are important for modelling the properties of molecular systems, similar to how mathematical functions are classified for finding solutions to differential equations. Molecular orbitals are formed by linear combinations of atomic orbitals using these basis sets. In this way, the system’s energy state, geometry, and other chemical properties can be calculated. Molecular orbitals are linear combinations of atomic orbitals. This linear combination shows how different atomic orbitals

combine in a specific molecule. The basis sets, on the other hand, are a set of functions consisting of the atomic orbitals used to form these molecular orbitals. Basic sets play a crucial role in calculating the molecular structures and properties. Since molecular orbitals are formed by combinations of atomic orbitals, the quality of the chosen basis set directly affects the accuracy of the results obtained. Therefore, choosing an appropriate basis set in quantum chemical calculations is critically important for accurately determining molecular properties. In molecular calculations, Slater-type orbitals (STO) or Gaussian-type orbitals (GTO) are commonly used. Both types are commonly preferred in the representation of atomic orbitals. Basis sets in quantum chemistry play a significant role in computational modelling. These are: Minimal Basis Set: Minimal basis sets contain the minimum number of atomic orbital basis functions necessary to describe a molecule. For example, in the STO-3G basis set, a representation similar to Slater-type orbitals is obtained by using three Gaussian-type orbitals for each atomic orbital. A minimal basis set is the simplest basis set containing the core orbitals of an atom. It usually only contains s and p orbitals.

2.6. Geometric Optimisation

Molecular geometry optimisation is an important process used to find the most stable configuration of a molecule. In this process, the minimum energy points of the potential energy surface are identified. In the first step, the gradient vector of the molecule's energy function is calculated. The gradient vector indicates the slopes and directions on the energy surface; therefore, when this vector is zero, it means the system has reached equilibrium. Points where the gradient vector is zero can often be minima, maxima, or a transition state (high energy). However, in molecular geometry optimisation, minimum energy positions are primarily of interest. Therefore, methods such as second derivative tests or energy calculations are used to determine which points among those with a gradient of zero are minima. These minimum energy states represent the most stable geometric configuration of the molecule, and this structure is a critical factor influencing the molecule's physical and chemical properties. Geometric optimisation explores the minima on the potential energy surface to determine the equilibrium structures of molecular sys-

tems. At minimum and saddle points, the first derivative of energy, i.e., the gradient, is zero; therefore, these points are considered stable structures. Geometry optimisation starts with an initially determined molecular geometry and progresses on the potential energy surface by calculating the energy and gradient at each step. The optimisation process continues with calculations based on the initial geometry. At each stage, optimisation is considered complete when the system's gradient vector is zero and the difference between the calculated geometries reaches a negligible level. At this stage, stable points are identified and evidence is provided that the molecule has reached its lowest energy state. Thus, the most stable geometric configuration affecting the physical and chemical properties of the molecule is obtained. Various optimisation algorithms used in this process can be adjusted according to specific tolerance levels, which can affect the computation time and accuracy.

2.7. Binding Energy

Binding energy (Eint) is the energy of the bond structure between particles in a system; in complex structures, it is calculated as the difference between the total energy of the complex and the sum of the energies of the isolated ligand and metal ion. Mathematically expressed as:

$$E_{int} = E_{complex} - (E_{ligand} + E_{metal\ ion})$$

Here, Eint represents the binding energy of the ligand, Ecomplex represents the total energy of the complex, Eligand represents the energy of the isolated ligand, and Emetal represents the energy of the isolated metal ion. The nature and strength of the interaction between the Eint, Eligand, and metal ions is an important criterion for determining the nature and strength of the interaction. This value indicates how stable or strong the interaction is.

A large negative binding energy value indicates that the corresponding interaction state is thermodynamically more stable. In short, a negative value indicates that the metal binds more thermodynamically to the chitosan surface or that the metal interacts with chitosan. In such a system, the binding energy can vary depending on the nature and intensity of the interactions between the chitosan surface and

the metal atoms (Natsir et al., 2022).

2.8. Energy Difference and Electronic Properties

The Highest Occupied Molecular Orbital (HOMO) and Lowest Unoccupied Molecular Orbital (LUMO) are important in determining the key electronic properties of molecular systems. In HOMO-chemical reactions, the ability to donate electrons is an indicator of the LUMO's ability to accept electrons in chemical reactions. FMO (Frontier Molecular Orbital) means "frontier molecular orbital" in chemistry and refers to the HOMO and LUMO orbitals. FMO theory is used to understand how molecules behave in chemical reactions and how their electrons interact. The HOMO-LUMO energy difference (or energy gap) is important in determining a molecule's chemical reactivity, optical properties, and electron conductivity. If the HOMO-LUMO energy gap is large, this generally indicates that the molecule has a stable structure and is less reactive. This is because a larger range indicates that the molecule is less responsive to external influences (such as redox or photon absorption) and undergoes less chemical change.

If the HOMO-LUMO gap is small, this generally indicates that the molecule is more reactive and can undergo chemical change more easily. A smaller band gap indicates that the molecule is more responsive to external influences and is therefore more reactive. FMO (Frontier Molecular Orbital) values are important for understanding intramolecular energy transfer and reaction mechanisms within the biological systems in which a molecule is located. Therefore, the analysis of FMO values is widely used in areas such as drug design and understanding biological interactions (Padmaja et al., 2009; Sagdınc & Pir, 2009).

3. Theoretical Methodology

In order to gain a deeper understanding of the molecular geometry and electronic structure, the compound was subjected to theoretical optimization using both Density Functional Theory (DFT) and Hartree–Fock (HF) methods. All calculations were carried out employing the 6-31++G(d,p) basis set, which offers a reliable balance

between computational efficiency and accuracy, particularly for organic molecules containing heteroatoms (Dennington, Keith & Millam, 2007).

The initial molecular geometry was obtained from previously reported single-crystal X-ray diffraction data. Subsequent geometry optimization was performed in the gas phase without imposing any symmetry constraints. The comparison of bond lengths, bond angles, and dihedral angles between the experimental (XRD-based) and theoretically optimized structures demonstrated a high degree of consistency, confirming the validity and reliability of the chosen computational models.

The observed agreement between experimental and calculated geometrical parameters validates the adequacy of both DFT and HF methods in accurately reproducing the molecular structure. These results not only support the crystallographic data but also provide a solid foundation for further theoretical investigations such as MEP mapping, frontier orbital analysis, and intermolecular interaction profiling.

3. 1. Molecular Electrostatic Potential (MEP) Analysis

Molecular electrostatic potential (MEP) mapping is a valuable theoretical approach to visualizing charge distribution across the molecular surface, allowing the identification of electrophilic and nucleophilic regions. This type of surface mapping aids in the prediction of non-covalent interactions, reactivity sites, and crystal packing behavior of molecular systems Thul, Gupta, Ram & Tandon, 2010).

In the generated MEP map of the studied compound, the electron-rich regions (red zones) correspond to the C=O atoms with a minimum potential of –0.043 a.u., suggesting their potential role as electrophilic interaction centers. These findings are in excellent agreement with previous studies that similarly localized the most negative potentials on carbonyl or nitro oxygen atoms. Furthermore, secondary red areas were observed around the $–NH_2$ group, indicating the presence of lone pair electrons on the nitrogen, which may engage in hydrogen bonding or dipolar interactions (Fig. 2).

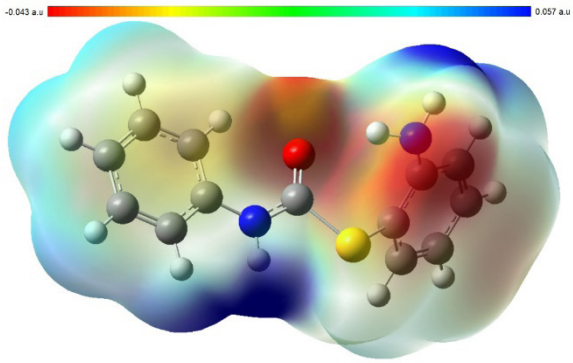

Figure 2. MEP shape of the title molecule.

Conversely, the most positive regions (blue zones), with a maximum of +0.057 a.u., are concentrated near C–H bonds, a finding consistent with the electropositive nature of hydrogen atoms and often noted in comparable systems (Gümüs et al., 2018).

These results support the electrostatic complementarity observed in the crystal structure, with negative and positive regions aligning in ways that stabilize molecular packing. The observed distribution strongly aligns with similar Schiff base and heterocyclic compounds previously reported in the literature (Bülbül, Atalay & Ertürk, 2023).

Thus, the MEP surface not only maps reactive tendencies but also reinforces the role of these electrostatic regions in stabilizing the molecular conformation and crystal architecture.

3.2. Frontier Molecular Orbital Analysis

Frontier molecular orbital (FMO) theory is a widely used framework for interpreting the electronic properties and chemical reactivity of molecules. The highest occupied molecular orbital (HOMO) and lowest unoccupied molecular orbital (LUMO) energies, as well as the gap between them (ΔE), are particularly informative indicators of a molecule's kinetic stability, electronic excitation potential, and reactivity trends.

In the present study, the HOMO energy of the molecule was calculated as −5.85 eV, and the LUMO energy as −1.02 eV, resulting in a HOMO–LUMO energy gap (ΔE) of 4.83 eV. This relatively moderate gap suggests that the molecule is electronically stable, yet capable of undergoing charge transfer processes under suitable con-

ditions (Fig. 3).

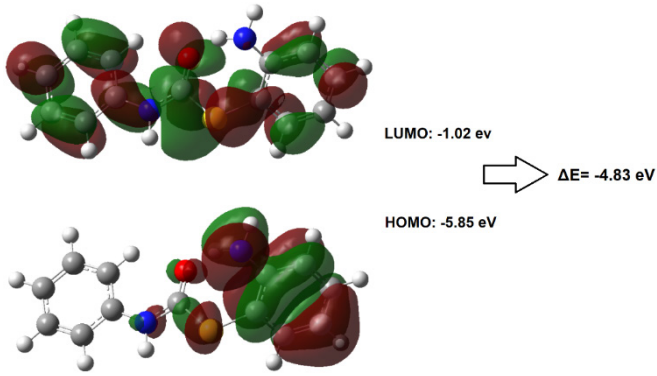

Figure 3. Molecular orbital energy levels of title compound.

The HOMO is generally associated with the ability to donate electrons, while the LUMO is associated with the ability to accept electrons. The spatial distribution of these orbitals plays a crucial role in determining the molecular reactivity. Visual inspection of the molecular orbital surfaces (Figure X) shows that:

The HOMO is mainly localized over the π-system and electronegative substituent regions, suggesting that these parts of the molecule are the most likely to participate in electron donation or be susceptible to oxidation.

The LUMO is distributed over the electrophilic regions, particularly near electron-withdrawing groups, which may act as sites for nucleophilic attack or reduction reactions.

This electronic arrangement supports the potential of the molecule to participate in intramolecular charge transfer (ICT) phenomena, which is important in the context of nonlinear optical (NLO) properties, chemical sensing, and pharmaceutical applications.

The calculated energy gap is in good agreement with previous reports on similar Schiff base and heterocyclic structures (Fukui, 1982; Tanak, 2011) confirming the consistency of the molecular design and its possible functional implications.

3.3. Hirshfeld Surface Analysis

Hirshfeld surface analysis is a powerful computational tool that provides insight into the nature and strength of intermolecular interactions within a crystal structure. This method enables the visualization and quantification of close contacts, thereby elucidating key non-covalent interactions that contribute to the overall stability and packing of the crystalline lattice.

In the present study, the normalized contact distance (dnorm) values were found to range from −0.4794 to 1.1656, indicating the presence of both close contacts (negative dnorm, shown in red regions) and longer-range, less interactive contacts (positive dnorm, shown in blue regions). The di (distance from the surface to the nearest nucleus inside the surface) ranged from 0.8139 Å to 2.5557 Å, and de (distance from the surface to the nearest nucleus outside the surface) varied between 0.8146 Å and 2.5397 Å. These ranges reflect a wide distribution of contact distances within the crystal lattice, typical for organic molecules exhibiting a complex network of weak intermolecular forces (Fig. 3).

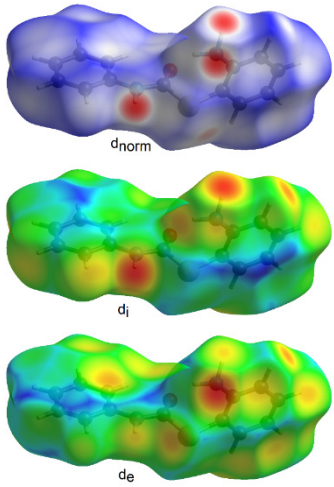

Figure 4. d_{norm}, d_i and d_e surfaces view of the title compound.

The 2D fingerprint plots revealed the relative contributions of various intermolecular interactions to the total Hirshfeld surface. The H···H contacts dominate the interaction landscape with a contribution of 44.1%, highlighting the significance of van der Waals-type hydrogen interactions in crystal packing. The second most prevalent

interaction is C···H/H···C (29.1%), followed by O···H/H···O (9.8%), which suggests the presence of moderate hydrogen bonding involving electronegative oxygen atoms (Fig. 4).

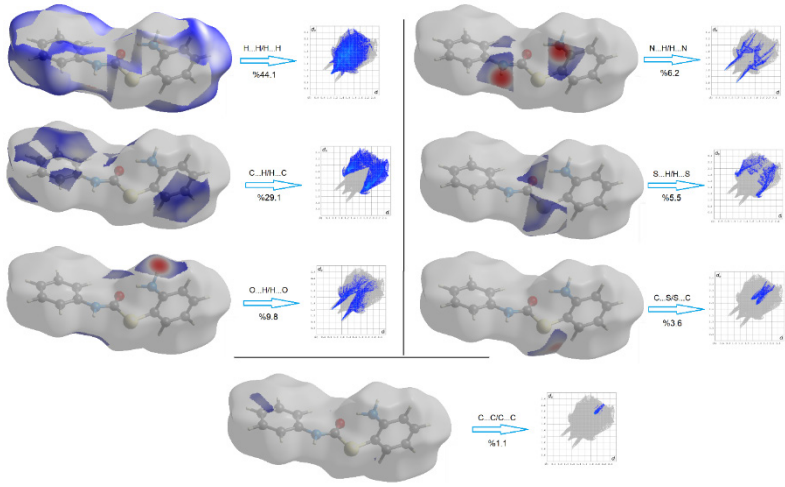

Figure 5. Interactions that contribute to the total Hirshfeld surface for title compound.

Other notable contributions include N···H/H···N (6.2%), S···H/H···S (5.5%), and C···S/S···C (3.6%) interactions, indicating that both nitrogen and sulfur-containing moieties participate in weak, yet significant, polar interactions. The C···C (1.1%) contacts were relatively minor, suggesting that π–π stacking is not a prominent feature in the crystal structure (Fig. 5).

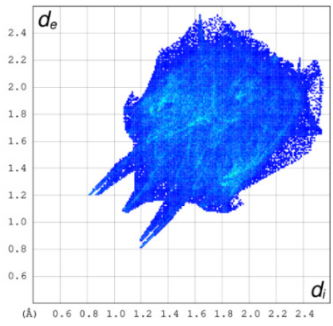

Figure 6. 2D fingerprint representation of the title compound.

These results are in good agreement with previously reported Hirshfeld analyses of structurally related molecules (Spackman & Byrom, 1997; Bülbül et al., 2024; Pasha et al., 2021), confirming the role of hydrogen-mediated interactions in stabilizing the solid-state conformation of the compound.

4. DISCUSSION AND CONCLUSION

To support the experimental results, the geometric parameters were calculated by using the DFT method and compared with the X-ray results. The theoretically calculated values of both geometric parameters of the structure of the minimum energy were investigated and then compared with X-ray crystallographic data. The theoretical results of the geometric parameters are successfully represented experimental data According to stability of the molecule to softness means that the molecule with least HOMO–LUMO gap and it means that it is more reactive molecule. MEP, Mulliken population analysis, NPA results are consistent with each other related to chemically reactivities of molecule. Natural bond orbital (NBO) calculations reveal the delocalization and hyperconjugation interaction, intramolecular charge transfer and stabilizationenergy of molecule. We hope the results of this study will help researchers to design and synthesis new metal materials.

REFERENCES

Becke, A.D. (1993). Density Functional Thermo chemistry III., The role of exact Exchange, Journal of Chemical Physics, 98, 5648.

Belkhir, K., Shen, H., Chen, J., Jegat, C. & Taha, M. (2015). Synthesis of multi-thiol functionalized polylactic acid, polyhydroxybutyrate and polycaprolactone, Eur. Polym. J. 66, 290–300.

Bülbül, H., Atalay, Ş., & Ertürk, A. G. (2023). Synthesis, spectroscopic characterizations, and comparison of experimental, and theoretical results of N-(3-chloro-2-methyl phenyl)-2-(4-methoxybenzylidene) hydrazine-1-carbothioamide. Journal of Molecular Structure, 1291, 136002.

Bülbül, H., Cetin, G., Köysal, Y., Şimşek, R., Öztürk Yıldırım, S., Tanak, H., & Butcher, R. J. (2024). Synthesis, crystal structure, spectroscopy and quantum chemical investigations of hexahydroquinoline molecule. Molecular Physics, 122(18), e2320784.

Chermette, H., (1998). Density functional theory: A powerful tool for theoretical studies in coordination chemistry. Coordination Chemistry Reviews, 178– 180, 699–721.

Dennington R, Keith T & MillamJ,GaussView, Version 4.1, Semichem, (Shawnee Mission, Kan, USA) 2007.

Doğan,Ş.D., Çetinkaya, Y., Buran, S., Yıldırım, S. & , Butcher, R.J. (2020). Chemoselective synthesis, X-ray characterization and DFT studies of new organic single crystal: S-(2-aminophenyl) cyclohexylcarbamothioate, Journal of Molecular Structure , 1204 (15) 127499.

Dorsett, H. & White, A., (2000). Overview of Molecular Modelling and Ab initio Molecular Orbital Methods Suitable for Use with Energetic Materials. Defence Scienceand Technology Organisation, 36p, Australia.

Frisch, M. J., Trucks, G. W., Schlegel, H.B., Scuseria, G. E., Robb, M. A., Cheeseman, J. R., Scalmani, G., Barone, V., Mennucci, B., Petersson, G. A., Nakatsuji, H., Caricato, M., Li, X., Hratchian, H. P., Izmaylov, A. F., Bloino, J., Zheng, G., Son-

nenberg, J. L., Hada, M., Ehara, M., Toyota, K., Fukuda, R., Hasegawa, J., Ishida, M., Nakajima, T., Honda, Y., Kitao, O., Nakai, H., Vreven, T., Montgomery, J. A., Jr., Peralta, J. E., Ogliaro, F., Bearpark, M., Heyd, J. J., Brothers, E., Kudin, K.N., Staroverov, V. N.,Kobayashi, R., Normand, J., Raghavachari, K., Rendell, A., Burant, J.C., Iyengar, S. S., Tomasi, J., Cossi, M., Rega, N., Millam, J. M., Klene, M., Knox, J.E., Cross, J. B., Bakken, V., Adamo, C., Jaramillo, J., Gomperts, R., Stratmann, R. E., Yazyev, O., Austin, A. J., Cammi, R., Pomelli, C., Ochterski, J. W., Martin, R. L., Morokuma, K., Zakrzewski, V. G., Voth, G. A., Salvador, P., Dannenberg, J. J., Dapprich, S., Daniels, A. D., Farkas, Ö., Foresman, J. B., Ortiz, J. V., Cioslowski, J. & D.J. Fox. (2009). Gaussian 09, Gaussian Inc., Wallingford CT.

Fukui K (1982) Role of frontier orbitals in chemical reactions, Science, 218(4574):747–754

Gümüs¸ MK, Kansız S, Aydemir E, Gorobets NY, Dege N (2018) Structural features of 7-methoxy-5-methyl-2-(pyridin-3-yl)-11, 12-dihydro-5, 11-methano [1, 2, 4] triazolo [1, 5-c] [1, 3, 5] benzoxadiazocine: Experimental and theoretical (HF and DFT) studies, surface properties (MEP, Hirshfeld). J Mol Struct, 1168:280–290.

Jensen, F. (1999). Introduction to Computational Chemistry, John Wiley and Sons Ltd., 26-38.

Kohn, W.& Sham, L.J., (1965). Self-Consistent Equations Including Exchange and Correlation Effects, Physical Review, 140 (4A), 1133-1138.

Natsir, M. A., Zam Zam, Z., Muin, F. & Umar, S. (2022). Analysis of Ni2+ Metal Adsorption on Chitosan Membrane Using Density Functional Theory, TECHNO: Jurnal Penelitian, 11(1), 63-70.

Öztürk Yıldırım, S. & Butcher, R.J.(2018). S-2-aminophenyl N-phenylcarbamothioate, IUCrData, 3, 180062.

Padmaja, L., Kumar, C. R., Sajan, D., Joe, I.H., Jayakumar, V.S. & Pettit, G.R., (2009). Density functional study on the structural conformations and intramolecular charge transfer from

the vibrational spectra of the anticancer drug combretastatin-A2, Journal of Raman Spectroscopy. 40, 419–428.

Pasha A R, Khalid M, Shafiq Z, Khan M U, Naseer M M, Tahir M N & Jawaria R. (2021). A comprehensive study of structural, non-covalent interactions and electronic insights into N-aryl substituted thiosemicarbazones via SC-XRD and first-principles DFT approach, J Mol Str, 1230, 129852.

Sagdınc S. & Pir H., (2009). Spectroscopic and DFT studies of flurbiprofen as dimer and its Cu(II) and Hg(II) complexes, Spectrochim. Acta A 73, 181–187.

Spackman, M.A. & Byrom, P.G. (1997). A novel definition of a molecule in a crystal, Chem. Phys. Lett. 267, 215–220.

Tanak, H. (2011). Crystal structure, spectroscopy, and quantum chemical studies of (E)-2-[(2-Chlorophenyl) iminomethyl]-4-trifluoromethoxyphenol. The Journal of Physical Chemistry A, 115(47), 13865-13876.

Thul, P., Gupta VP, Ram VJ & Tandon P.(2010) Spectrochimica Acta Part A: Molecular and Biomolecular Spectroscopy, Structural and spectroscopic studies on 2-pyranones, 75(1), 251-260.

Torrico-Vallejos, S., Erben, M. F., Hey-Hawkins, E. & Della Ve´dova, C. O. (2011). Tetrahedron Lett. 52, 5352–5354.

Young, D.C., (2001). Computational Chemistry A Practical Guide for Applying Techniques to Real-World Problems (Electronics). John Wiley and Sons, 381p, New York.

Yıldırım Öztürk, S., Büyükmumcu, Z., Doğan, Ş. D. & Butcher R. J. (2018). Redetermination and density functional studies of N,N'xx-(disulfanediyldibenzene-2,1-diyl)dipyridine-2-carboxamide, Journal of Structural Chemistry, cilt.59, sa.8, ss.1861-1867.

Yıldırım Öztürk, S., Büyükmumcu, Z. Savaş Pekdur, Ö., Butcher, R.J. & Doğan, Ş.D. (2018). Structural and spectral analyses ofN,N'-(2,2'-dithiodi-o-phenylene)bis-(furan-2-carboxamide), AIP Conf. Proc. 1935, 040002.

Chapter 5

REMOVAL OF NI (II) IONS FROM AQUEOUS SOLUTION USING PERSIMMON (DIOSPYROS KAKI L.) LEAVES POWDER: ADSORPTION KINETICS, ISOTHERM, AND THERMODYNAMICS STUDY)[1]

Melike KALE[2], Yunus Emre ŞİMŞEK[3]

1 This article is extracted from Melike Kale's master's thesis "Biyokütle Kullanılarak Metal İyon Biyosorpsiyonu", supervised by Yunus Emre Şimşek (Master's Thesis, Bilecik Şeyh Edebali University and Anadolu University, Institute of Science, Reference No: 10194118, Bilecik, Türkiye, 2018). This work was supported by Bilecik Şeyh Edebali University Research Projects Coordination Unit under Grant No. 2017-01. BŞEÜ.03-10.

2 MSc., Quality Insurance Manager, Hepşen Metal ve Bileşenleri Paz. San. ve Tic. A.Ş., TR 11100 Bilecik, Türkiye, kalite@hepsenkimya.com.tr, ORCID: 0009-0008-7380-9720

3 Assist. Prof. Dr. Bilecik Seyh Edebali University, Faculty of Engineering, Department of Chemical Engineering, TR 11100 Bilecik, Türkiye, yunusemre.simsek@bilecik.edu.tr, ORCID: 0000-0001-6722-2052

1. INTRODUCTION

In recent years, industrial and urban waste have increased, as expected, due to the growing population and increasing industrialization. Agriculture and forestry, automotive, mining, fertilizer and pesticide, electroplating and paint, fossil fuel plants, and other industries generate heavy metal wastes, which are one of the leading causes of environmental pollution when released into water bodies without proper control. Heavy metals include elements such as cadmium, mercury, lead, chromium, nickel, copper, and arsenic, which have a density exceeding 4.5 g/cm³ [Mei et al., 2025]. If these metals leak into water even in trace amounts, they have severe effects on humans, flora, and fauna [Soni et al., 2025].

There are various treatment methods, such as chemical precipitation [Tsai et al., 2020], electrocoagulation [Boulanour et al., 2025], electroflocculation [Hadikhani et al., 2024], microbial degradation [Sharma et al., 2024], photo-electrocoagulation-oxidation [Shahedi et al., 2025], membrane filtration [Tian et al., 2025], ion exchange [Aberdeen et al., 2025], and adsorption [Huang et al., 2022] to remove nickel Ni (II) from aqueous media.

Adsorption holds a privileged position in wastewater treatment due to its simplicity of application, high removal efficiency for different types of contaminants, cost effectiveness, regenerability, and non-toxicity, which can be employed to remove heavy metal ions, nitrate, phosphate, dyes, organic and inorganic compounds, pathogens, and pesticides from aqueous solutions [Huang et al., 2022]. Several factors affect the adsorption process, including adsorbent dosage, pH, temperature, contact time, and initial heavy metal concentration. Moreover, the properties of the adsorbent material also influence the metal removal efficiency, including the species of the adsorbent, its physicochemical properties, and any pretreatment of the raw material, such as the method of activation, physical and chemical modification, and immobilization [Ross et al., 2021]. Various types of materials have been reportedly used for adsorbents, among which are agricultural wastes, algae, fungus, and their residues, nanocomposites, metal (oxy-hydro) oxides, clay minerals, bio-polymer-based substrates, biochars, activated carbons, and tree/plant leaves [Saod et al., 2025; Mei et al., 2025; Martha et al., 2020; Islam et al., 2019]. The leaves of many tree and plant species have been

used directly as adsorbents or as precursors for producing biochar via chemical and/or physical activation techniques to remove heavy metal ions from aqueous media.

Vilvanathan and Shanthakumar reported that teak (Tectona grandis) plant leaf powder could remove nickel ions from a synthetic heavy metal solution with an adsorption capacity of 17.81 mg/g [Vilvanathan and Shanthakumar, 2016]. Gutha et al. investigated the ability of the adsorbent prepared from tomato (Lycopersicum esculentum) leaves. They studied the effect of adsorption parameters, i.e., solution pH, adsorbent dosage, initial metal concentration, and contact time. The maximum adsorption capacity for Ni(II) was found to be 58.82 mg/g [Gutha et al., 2015]. In another study [Kumar and Kirthika, 2009], bael tree leaf powder was used to study the adsorption capacity of Ni(II) through batch experiments. The adsorption experiments revealed that the adsorption capacity and removal efficiency were 1.527 mg/g and 60.21%, respectively, under optimal conditions: an adsorbent dosage of 20 g/L, an initial heavy metal concentration of 10 mg/L, a pH of 6.2, and a temperature of 30 °C.

Diospyros, belonging to the Ebenaceae family, is a woody tree with over 250 species. It is widely distributed in the tropics and subtropics. Fruit-bearing Diospyros species such as Diospyros kaki, Diospyros Virginiana, Diospyros digyna, Diospyros lotus, and Diospyros rhombifolia are commercially important. Diospyros kaki is the cultivated species of the genus *Diospyros*. It is a sparsely branched deciduous tree that sheds its leaves in winter. Fruit formation begins in September and October while the leaves are still present, and the fruits ripen after the leaves fall. Seasonal fruits are rich in minerals, fiber, phenolic compounds, and bioactive compounds. The leaves are ovate-elliptical, 5–18 cm long and 2.8-9 cm wide, glossy dark green on the upper surface, and hairless on the lower surface. Diospyros leaves have been utilized in folk medicine, beverages, personal care products, and food industries [Murali et al., 2023; Khumaidi et al., 2023; Rauf et al., 2017; Xie et al., 2015]. Plant and tree leaves consist mainly of cellulose, hemicellulose, and lignin compounds. Wang et al. [Wang et al., 2004] reported that Diospyros kaki leaves contain cellulose 68.28%, hemicellulose 7.54%, and lignin 11.70%. Besides these main chemical compounds, the leaves of Diospyros species also contain flavonoids, tannins,

terpenoids, and other compounds such as carotenoids, coumarins, steroids, naphthoquinones, and fatty and organic acids [Khumaidi et al., 2025; Kashif et al., 2017]. In the literature, studies on Diospyros species primarily focus on their nutraceutical and pharmacological properties. However, studies on the use of Diospyros as an adsorbent in environmental applications are highly limited. Galera et al. [2024] investigated the usability of leaf powder produced from Diospyros kaki as an adsorbent for the removal of Cu(II) and Cd(II) heavy metal ions from aqueous solutions. The maximum adsorption capacities were found to be 0.213 mmol/g and 0.215 mmol/g for Cu(II) and Cd(II), respectively.

In this study, the removal efficiency of Ni(II) through batch-mode adsorption using Persimmon tree leaf powder (PTLP) as an adsorbent was thoroughly investigated. Key adsorption parameters, including solution pH, adsorbent dosage, contact time, and initial heavy metal concentration, were optimized to maximize adsorption capacity. Moreover, comprehensive characterization analyses of the adsorbent were conducted to evaluate its structural, chemical, and morphological properties. Additionally, adsorption kinetics, isotherms, and thermodynamic studies were conducted under the optimized adsorption conditions.

2. MATERIALS AND METHODS

2.1 Chemical Reagents

Sodium hydroxide (NaOH, 99%), hydrochloric acid (HCl, 37%), and nickel (II) nitrate hexahydrate ($Ni(NO_3)6H_2O$, >99.99) were purchased from Merck and used without further purification. A certain amount of $Ni(NO_3).6H_2O$ was dissolved in ultrapure water to prepare a stock standard solution of 1000 ppm of Ni(II). The initial pH value of heavy metal solutions was adjusted with 0.1 M (HCl) and 0.1 M (NaOH) solutions.

2.2 Preparation of Adsorbent

The leaves of persimmon (PTLP) were collected in the province of Bilecik, Türkiye, for Ni(II) heavy metal removal. The raw material was washed with ultra-pure water to remove dust and other contaminants before the adsorption experiments. It was then oven-

dried at 105 °C for 48 hours, ground using a hand blender, and sieved to a particle size of approximately 0.150 mm.

2.3 Experimental Procedure

Adsorption experiments were carried out by batch adsorption methods using 100 mL conical flasks of 50 mL containing heavy metal ions at 500 rpm continuous mixing rate at different adsorption parameters i.e., at temperature (20-40 °C), pH (1.5 to 7), adsorbent dosage (0.0025 to 0.5 g), contact time (5 to 180 min), and heavy metal concentration (25 to 200 ppm). The effects of initial pH, adsorbent dosage, contact time, and initial nickel concentration were investigated by varying one parameter while keeping the others constant. Nickel concentrations were determined by Perkin Elmer A900 Atomic Absorption Spectroscopy. In all experiments, nickel adsorption capacity (q, mg/g) and removal efficiency (R, %) were determined by the following equations (Eqs. 1-2), respectively.

$$Removal\ effciency, R\ (\%) = \frac{(C_0 - C_e)x100}{C_0} \quad (1)$$

$$Adsorption\ capacity, q\ (\frac{mg}{g}) = \frac{(C_0 - C_t)xV}{W} \quad (2)$$

Where C_0, C_e and $C_t(\frac{mg}{L})$ are the initial, equilibrium concentration, and concentration at any time t of Ni(II), respectively. $V\ (mL)$ is the volume of the heavy metal solution, and $W\ (g)$ is the mass of the adsorbent.

2.4 Adsorption Kinetic and Isotherm Models

The adsorption kinetic models are mathematical models used to determine the adsorption rate as a function of time. A detailed investigation into the adsorption kinetics of Ni(II) was conducted using nonlinear and linear pseudo-first-order (PFO), nonlinear and linear pseudo-second-order (PSO), nonlinear and linear Elovich, and nonlinear and linear intraparticle kinetic models. Adsorption isotherm models are employed to assess the adsorption mechanism

and the maximum adsorption capacity of the adsorbent. In this study, nonlinear and linear Langmuir, nonlinear and linear Freundlich, nonlinear and linear Temkin, and nonlinear and linear Redlich-Peterson adsorption models were used to evaluate adsorption isotherms. Table 1 presents the adsorption kinetic and isotherm models, along with their relevant parameters. Three distinct error analyses were employed to determine the adsorption mathematical models using experimental data by fitting the most appropriate kinetic and isotherm models: the coefficient of determination (R^2), adjusted coefficient of determination (Adj-R^2), and Chi-square (χ^2).

Table 1. Adsorption kinetic and isotherm models used in this study

Models	Nonlinear Form	Linear Form	Parameters
Kinetic models			
PFO	$q_t = q_e(1 - e^{-k_1 t})$	$\ln(q_e - q_t) = lnq_e - k_1 t$	q_e : Adsorption capacity at equilibrium (mg/g)
PSO	$q_t = \frac{k_2 q_e t}{(1 + k_2 q_e t)}$	$\frac{t}{q_t} = \frac{1}{k_2 q_e^2} + \frac{1}{q_e} t$	q_t: Adsorption capacity at any time t (mg/g)
Elovich	$q_t = \frac{ln(\alpha\beta t)}{\beta}$	$q_t = \beta \ln(\alpha\beta) + \ln(t)$	k_1 : First-order rate coefficient (L/min)
Intraparticle	$q_t = k_{id} t^{1/2} + C$		k_2 : Second-order rate coefficient (g/mg.min)
			k_{id} : Intra-particle diffusion rate coefficient (mg/min$^{-1/2}$)
			α : Initial adsorption rate (mg/g.min)
			β : Initial adsorption rate (mg/g.min)

Isotherm models			
Langmuir	$q_e = \frac{q_m K_L C_e}{1 + K_L C_e}$	$\frac{1}{q_e} = \frac{1}{q_m} + \frac{1}{q_m K_L C_e}$	q_e : Adsorption capacity at equilibrium (mg/g) q_m : Maximum adsorption capacity (mg/g) C_e : Concentration at equilibrium (mg/L) n_f : dimensionle"ss constant K_L: Langmuir isotherm constant (L/mg) K_F : Freundlich isotherm constant (mg/g)/(L/mg^{-1})$^{1/n}$ K_T : Temkin isotherm constant (L/g) β_T: heat of adsorption (J/mol); K_{RP} a_{RP} and n_{RP}: Redlich-Peterson isotherm constants
Freundlich	$q_e = K_F C_e^{(\frac{1}{n_F})}$	$\ln(q_e) = \ln(K_F) + \frac{1}{n_F}\ln(C_e)$	
Temkin	$q_e = \beta_T \ln(K_T C_e)$	$q_e = \beta_T \ln(K_T) + \beta_T \ln(C_e)$	
Redlich-Peterson	$q_e = \frac{K_{RP} C_e}{1 + a_{RP} C_e^{n_{RP}}}$	$\ln\left(K_{RP}\frac{C_e}{q_e} - 1\right) = n_{RP}\ln(a_{RP}) - K_{RP}\ln(C_e)$	

2.5 Adsorption Thermodynamic Studies

Solution temperature considerably affects the thermodynamic parameters of adsorption such as the Gibbs free energy change (ΔG°) (J/mol), enthalpy change (ΔH°) (J/mol), and entropy change (ΔS°) (J/mol K). To determine these parameters, the Ni(II) adsorption experiments were carried out at three different temperatures (293, 303, and 313 K). The Van't Hoff formula (Eq. 3) is used to find the ΔH° and ΔS°. It represents that a plot of $\ln K_d\ (\frac{q_e}{C_e}) = -\frac{\Delta H^\circ}{RT} + \frac{\Delta S^\circ}{R}$ versus $^1/_T$ must be a line with slope $-\frac{\Delta H^\circ}{R}$ and intercept $\frac{\Delta S^\circ}{R}$. Furthermore, ΔG° is determined by Eq. (4).

$$\ln K_d\ (\frac{q_e}{C_e}) = -\frac{\Delta H^\circ}{RT} + \frac{\Delta S^\circ}{R} \tag{3}$$

$$\Delta G^\circ = -RTlnK_d \tag{4}$$

2.6 Characterization of PTLP

The SEM-EDS system (SEM SEM-Zeiss Supra 40 Vp Gemini) was used to analyze the surface morphology and elemental content of PTLP. The functional groups of the material were determined by FTIR (Agilent Carry 630 FTIR Spectrometer). The specific surface area, pore size distribution, and pore size characteristics were analyzed by a fully automated BET Micrometric ASAP 2020 Plus Physisorption Analyzer. The surface charge of PTLP was measured with the Zeta Potential Analyzer (Malvern/Nano-ZS).

3. RESULTS AND DISCUSSION

3.1 Effect of Solution pH

The pH value of the heavy metal solution is one of the most critical parameters affecting the adsorption process. As shown in Fig. 1(a), the equilibrium adsorption of Ni(II) ions on the adsorbent increases with increasing pH values. For the solution pH values of 1.5, 2, 2.5, 3, 3.5, 4, 4.5, 5, 5.5, 6, 6.5, and 7, the adsorption capacities were 0.34, 0.99, 7.37, 11.48, 12.81, 14.01, 15.48, 17.09, 16.89, and 16.79

mg/g, respectively. These results reveal that at low pH values, the surface of the adsorbent becomes positive, owing to hydrogen exchange between the adsorbent and the heavy metal solution, which causes a decrease in the amount of Ni(II) ions. However, alongside increasing pH values, the adsorption capacity was enhanced due to the intermolecular attraction between the positively charged Ni(II) ions and the negatively charged adsorbent surface. The adsorption capacity remained almost unchanged after pH 5; therefore, the initial heavy metal concentration at pH 5 was used for further adsorption experiments.

3.2 Effect of Adsorbent Dosage

To evaluate the effect of adsorbent dosage on the removal efficiency of the adsorbent, the adsorbent dosage was varied, 0.025, 0.05, 0.1, 0.2, 0.3, and 0.5 g. The experiments were carried out under optimized pH conditions, as discussed in the previous section. Fig. 1(b) illustrates the effect of varying adsorbent dosage on the Ni (II) heavy metal ions. The removal efficiency increased with adsorbent dosage, which was found to be 54% at an adsorbent dosage of 0.2 g and reached a plateau after this value. This observation indicates that Ni (II) metal adsorption onto PTLP was almost directly proportional to the adsorbent dosage. A dosage of 0.2 g of adsorbent was used for the subsequent experiments.

Figure 1. Effect of (a) pH, (b) adsorbent dosage, (c) contact time, and (d) initial heavy metal concentration on adsorption capacity and removal efficiency

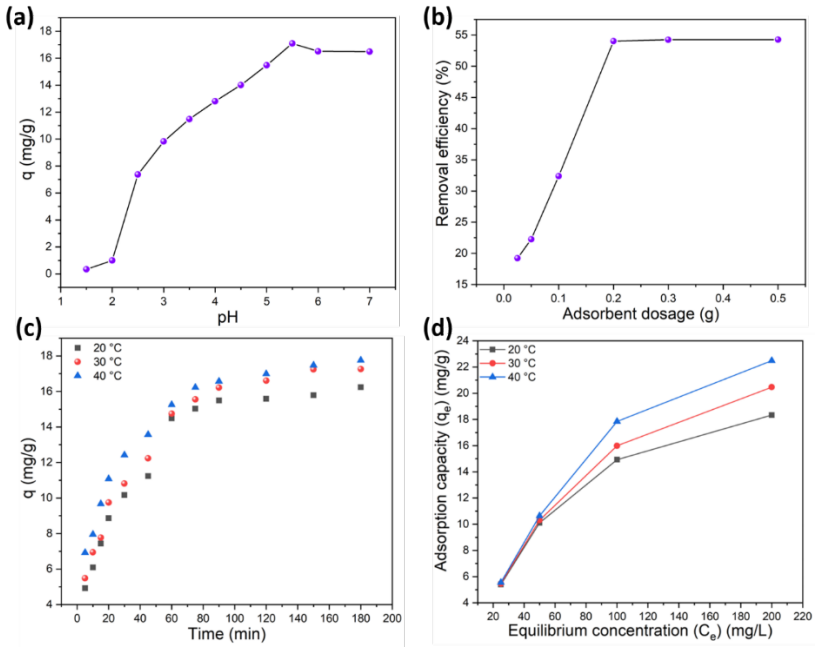

3.3 Effect of Contact Time and Temperature

To investigate the effects of contact time with nickel ions and the temperature of the heavy metal solution on the adsorbent capacity, adsorption experiments were conducted at 20, 30, and 40 °C with a pH of 5 and an adsorbent amount of 0.2 g. The adsorption capacity at 5, 10, 20, 25, 30, 50, 60, 80, 90, 120, 150, and 180 min for each temperature is shown in Fig. 1(c). At all temperatures studied, the most rapid adsorption occurred within 60 min, with the adsorption capacity of the adsorbent for Ni(II) increasing from 4.92, 5.48, and 6.92 mg/g to 15.90, 14.74, and 15.26 mg/g, respectively, for 20, 30, and 40 °C. As the contact time progressed, the adsorption rate steadily decreased. Eventually, the adsorption of Ni(II) ions reached equilibrium within 100 min, and the maximum adsorption capacity

for PTLP reached 16.24, 17.26, and 17.76 mg/g, for 20, 30, and 40 °C, respectively. Meanwhile, the adsorption capacity increased as the temperature rose. This phenomenon suggests that the adsorption of the metal ions was an endothermic process. The maximum adsorption capacity favors high solution temperature [Huang et al., 2022].

3.4 Effect of Initial Heavy Metal Concentration and Temperature

To study the effects of initial heavy metal concentration and solution temperature on the adsorption capacity, adsorption experiments were conducted at 25, 50, 100, 150, and 200 mg/L of initial heavy metal concentrations at 20, 30, and 40 °C, for a pH of 5, and with an adsorbent amount of 0.2 g. As presented in Fig. 1(d), with the increase in the initial heavy metal concentration and temperature, the adsorption of Ni(II) by PTLP gradually increased and attained surface saturation at high concentrations. This may be attributed to the abundance of active sites on the adsorbent surface, which are sufficient to hold the metal ions.

As the concentration of heavy metal increased, nearly all active sites were occupied by the metal ions, resulting in the maximum metal ion uptake. In this study, the maximum adsorption capacities of PTLP for Ni(II) were 18.33, 20.46, and 22.49 mg/g at solution temperatures of 20, 30, and 40 °C, respectively.

3.5 Adsorption Kinetic Studies

Exploring the adsorption kinetics is crucial because it provides valuable information on the adsorption mechanism, which is vital for determining adsorption as a function of contact time. In this research, four extensively used kinetic models — PFO, PSO, the Elovich, and intraparticle diffusion models —were employed to examine the kinetic data and determine the rate-determining step of Ni(II) adsorption on PTLP. The adsorption kinetic plots were prepared at different temperatures and contact times under optimized conditions

(pH 5, adsorbent dosage 0.2g, and initial heavy metal concentration 100 ppm). Figs. (2-3) illustrate the nonlinear and linearized forms of the aforementioned kinetic models, respectively. Moreover, the kinetic parameters of the models and error metrics are summarized in Tables 2 and 3. Considering the nonlinear kinetic models (Table 2), though PSP, intraparticle, and diffusion models fit the experimental data, the nonlinear PSO kinetic model describes the experimental data best with the highest values of R^2 of 0.9697-0.9834 and Adj-R^2 of 0.9663-0.9817, respectively, and the lowest values of χ^2 (0.5818-0.2686). Similarly, as presented in Table 3, the linearized PSO model is the most suitable one to describe the adsorption kinetics of Ni(II) onto PTLP for similar reasons. Furthermore, the calculated adsorption capacities values ($q_{e,(cal)}$) of 18.30, 19.24, and 19.83 mg/g, and 18.05, 19.25, and 19.06 mg/g by nonlinear and linear kinetic models, respectively at 20, 30, and 40 °C are good harmony with the experimental adsorption capacity values ($q_{e,(exp)}$) of 16.24, 17.26 and 17.95 mg/g for the temperatures of 20, 30, and 40 °C, respectively.

Figure 2. Effect of temperature on the kinetics of Ni(II) adsorption; non-linear adsorption kinetic models of PTLP at (a) 20 °C, (b) 30 °C, and (c) 40 °C

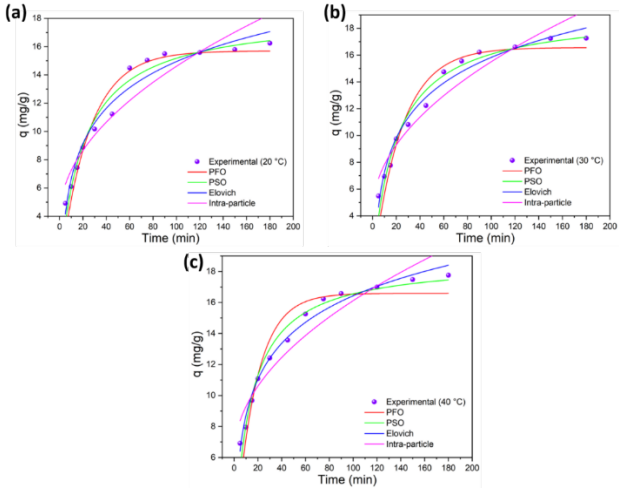

Figure 3. Effect of temperature on the kinetics of Ni(II) adsorption; (a) linear adsorption kinetic model PFO, (b) PSO, (c) Elovich, and (d) intra-particle diffusion models of PTLP at different temperatures

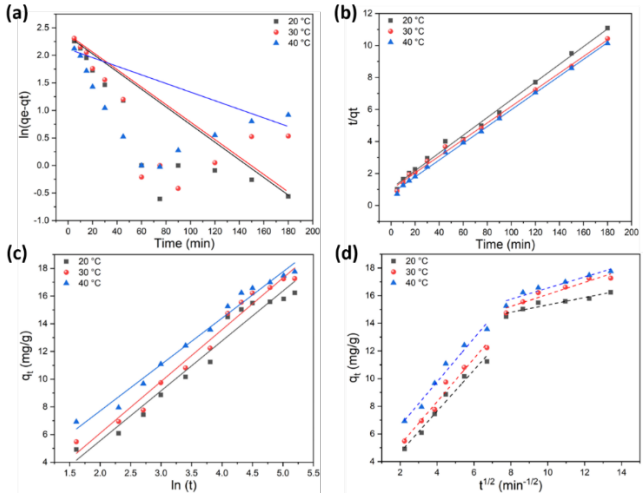

Table 2. Nonlinear pseudo first order, linear pseudo second order, Elovich, and intraparticle diffusion kinetic parameters of the adsorption Ni(II) onto RM with the variation of temperature, and calculated statistical metrics

Kinetic Models/Parameters	Temperature (°C)		
	20	30	40
Pseudo-first order			
k_1 (1/min)	0.0402	0.0414	0.0572
$q_{e,(exp)}$ (mg/g)	16.24	17.26	17.76
$q_{e,(cal)}$ (mg/g)	20.09	21.82	25.51
R^2	0.9484	0.9361	0.9018
Adj- R^2	0.9433	0.9267	0.8919
$\chi 2$	0.9888	1.2981	1.5896
Pseudo-second order			
k_2 (1/min)	0.0027	0.0026	0.0041
$q_{e,(exp)}$ (mg/g)	16.24	17.26	17.76
$q_{e,(cal)}$ (mg/g))	18.30	19.24	19.83
R^2	0.9697	0.9758	0.9834
Adj- R^2	0.9663	0.9734	0.9817
$\chi 2$	0.5818	0.4914	0.2686
Intraparticle diffusion			
K_{id} (mg/gmin$^{0.5}$)	1.0757	1.1240	0.9977
C_{id} (mg/g)	3.8524	4.2671	6.1387
R^2	0.8941	0.9218	0.9115
Adj- R^2	0.8836	0.9140	0.9027
$\chi 2$	2.0303	1.5876	1.4319
Elovich			
α (mg/gmin)	2.2797	2.5869	4.5325
β (g/mg)	0.2775	0.2677	0.2987
R^2	0.9613	0.9733	0.9703
Adj- R^2	0.9575	0.9706	0.9673

$\chi 2$	0.7417	0.5425	0.4806

Table 3. Linear pseudo-first order, pseudo-second order, Elovich, and intraparticle diffusion kinetic parameters of the adsorption Ni(II) onto RM with the variation of temperature, and calculated statistical metrics

Kinetic Models/Parameters	Temperature (°C)		
	20	30	40
Pseudo-first order			
k_1 (1/min)	0.0016	0.0017	0.0018
$q_{e,(exp)}$ (mg/g)	16.24	17.26	17.76
$q_{e,(cal)}$(mg/g)	7.09	7.56	5.51
R^2	0.8480	0.8604	0.8681
Adj- R^2	0.0707	0.0705	0.0723
$\chi 2$	9.2071	8.1341	7.9213
Pseudo-second order			
k_2 (1/min)	0.0034	0.0037	0.0027
$q_{e,(exp)}$ (mg/g)	16.24	17.26	17.76
$q_{e,(cal)}$ (mg/g))	18.05	19.25	19.06
R^2	0.9950	0.9965	0.9986
Adj- R^2	0.9945	0.9961	0.9984
$\chi 2$	0.0569	0.0351	0.0154
Intraparticle diffusion			
K_{id1} (mg/gmin$^{0.5}$)	1.4862	1.5594	1.5767
C_{id1} (mg/g)	1.6987	2.0929	3.4558
R^2	0.9767	0.9771	0.9724
Adj- R^2	0.9712	0.9713	0.9656
$\chi 2$			
K_{id2} (mg/gmin$^{0.5}$)	0.2661	0.4351	0.4029
C_{id2} (mg/g)	12.6618	11.7371	12.5159

R^2	0.9077	0.9188	0.9318
Adj- R^2	0.8847	0.8986	0.9147
$\chi 2$			
Elovich			
α (mg/gmin)	2.2810	2.5925	0.3013
β (g/mg)	0.2814	0.2714	4.5410
R^2	0.9612	0.9758	0.9400
Adj- R^2	0.9575	0.9734	0.9821
$\chi 2$	0.7410	0.4910	0.2714

3.6 Adsorption Isotherm and Thermodynamic Studies

The adsorption isotherm models expound the interaction between the adsorbate and adsorbent, clarifying the adsorption mechanism [Yin et al., 2024]. Numerous adsorption isotherm models have been reported in the literature. In this study, four widely used isotherm models — namely, the Langmuir, Freundlich, Temkin, and Redlich-Peterson models — were employed to analyze the experimental data. The adsorption plots were prepared at different temperatures and heavy metal concentrations under optimized conditions (pH 5, adsorbent dosage 0.2 g, and contact time 180 min). Fig. 4-5 depicts nonlinear and linearized forms of these models, respectively.

Figure 4. Non-linear adsorption isotherm Ni(II) onto PTLP (a) at 20 °C, (b) 30 °C, and (c) 40 °C, and (d) Van't Hoff plot for the adsorption of Ni(II) onto PTLP

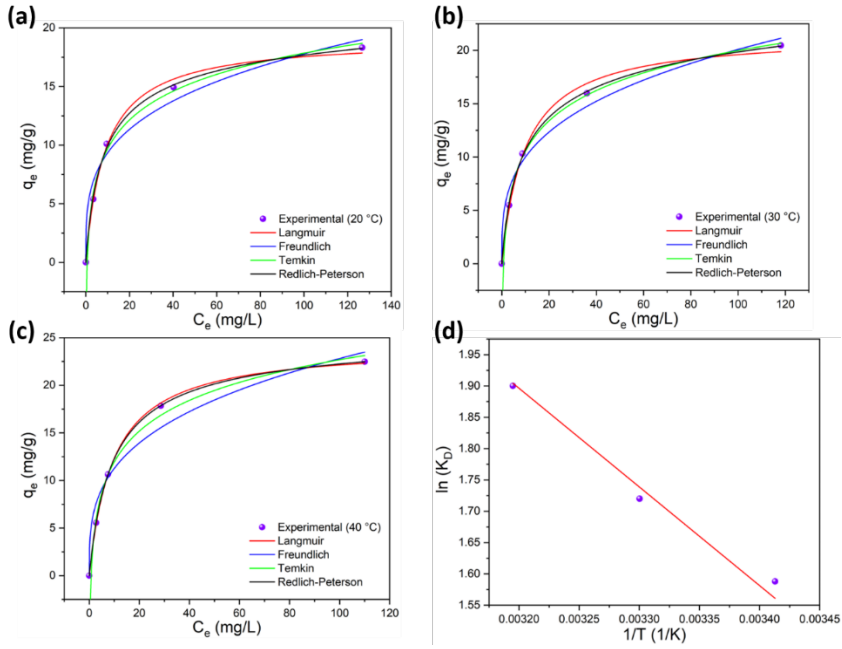

Figure 5. Linear adsorption isotherm models for Ni(II) onto PTLP at different temperatures (a) Langmuir, (b) Freundlich, (c) Temkin, and (d) Redlich-Peterson

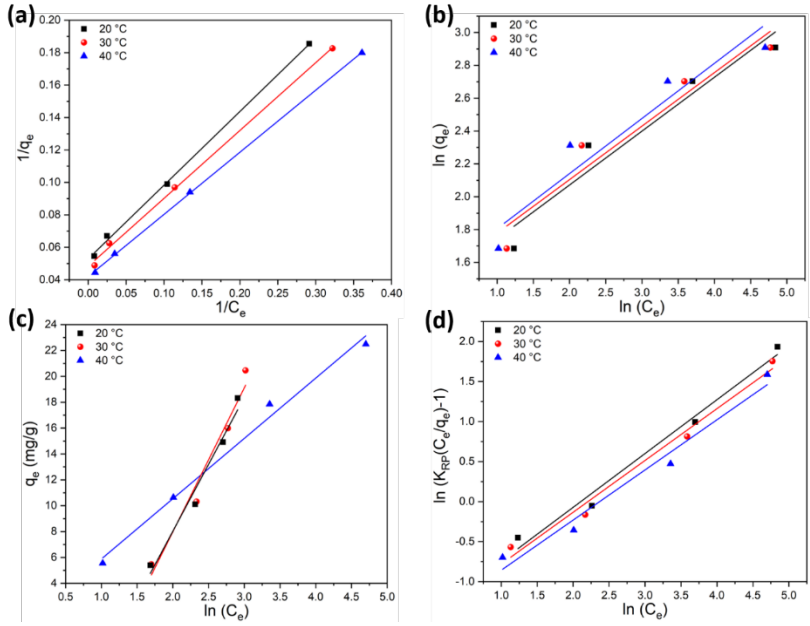

Table 4-5 lists the relevant isotherm parameters and statistical metrics. As presented in Table 4, the non-linear Langmuir isotherm model best suited the experimental data for all temperatures, with the highest R^2 values of 0.9949-0.9996 and adj-R^2 values of 0.9778-0.9994, and the lowest χ^2 values of 0.0015-0.1149. Likewise, the statistical metrics of the linearized Langmuir model fittings are in good harmony with those of the nonlinear results. The maximum adsorption capacity can be determined by the Langmuir isotherm model. The calculated adsorption capacity values ($q_{max, exp}$) of 19.12, 21.54, and 24.27 mg/g and 18.91, 20.68, and 23.81 mg/g at 20, 30, and 40 °C, respectively, by nonlinear and linear Langmuir isotherm models are in close agreement with the experimental adsorption capacity values of 18.25, 20.41, and 23.48 mg/g. These findings suggest that the adsorption of Ni(II) onto PTLP can be described by the Langmuir model. This model is based on the assumption that the active sites on the surface of the adsorbent are a monolayer and that

adsorption occurs without any interaction between adsorbed solute [Huang et al., 2022; Yin et al., 2024].

Table 4. Nonlinear Langmuir, Freundlich, Temkin, and Redlich-Peterson model adsorption parameters of the adsorption Ni(II) onto PTLP with the variation of temperature and calculated statistical metrics

	Temperature (°C)		
Isotherm Models/Parameters	**20**	**30**	**40**
Langmuir			
$q_{max,\ exp}$ (mg/g)	18.25	20.41	23.48
$q_{e,\ (cal)}$ (mg/g))	19.12	21.54	24.27
K_L (L/mg)	0.1113	0.1009	0.1034
R^2	0.9983	0.9949	0.9996
Adj- R^2	0.9778	0.9991	0.9994
$\chi 2$	0.1149	0.0444	0.0015
Freundlich			
K_F ((mg/g)(L/mg)$^{1/n}$)	4.9071	4.9771	5.5687
n_F	3.5759	3.3001	3.2658
R^2	0.9775	0.9817	0.9678
Adj- R^2	0.9770	0.9756	0.9571
$\chi 2$	1.6078	1.6183	3.5305
Temkin			
β_T (J/mol)	3.5466	4.0984	4.6629
K_T (L/g)	1.5336	1.3119	2.7401
R^2	0.9966	0.9933	0.9991
Adj- R^2	0.9952	0.4439	0.9990
$\chi 2$	0.2605	0.0831	0.0488

Redlich-Peterson			
a_{RP}	0.2058	0.2362	0.9638
n	0.9202	0.8891	0.9638
K_{RP}	2.6954	3.0119	2.7401
R^2	0.9963	0.9940	0.9991
Adj- R^2	0.9950	0.9989	0.9991
$\chi 2$	0.2667	0.0726	0.0018

Table 5. Linear Langmuir, Freundlich, Temkin, and Redlich-Peterson model adsorption parameters of the adsorption Ni(II) onto PTLP with the variation of temperature and calculated statistical metrics

Isotherm Models/Parameters	**Temperature (°C)**		
	20	**30**	**40**
Langmuir			
$q_{max,\ exp}$ (mg/g)	18.25	20.41	23.48
$q_{e,\ (cal)}$ (mg/g))	18.91	20.68	23.81
K_L (L/mg)	0.1165	0.1156	0.1097
R^2	0.9987	0.9985	0.9998
Adj- R^2	0.9981	0.9976	0.9997
$\chi 2$	0.0010	0.0011	0.0001
Freundlich			
K_F ((mg/g)(L/mg)$^{1/n}$)	4.1182	4.640	4.4059
n_F	3.0485	2.8314	2.6753
R^2	0.9344	0.9494	0.9338
Adj- R^2	0.9016	0.9122	0.8988
$\chi 2$	0.0285	0.0254	0.0382

Temkin			
β_T (J/mol)	10.3451	11.1295	4.6629
K_T (L/g)	1.7624	2.3326	1.2972
R^2	0.9719	0.9667	0.9907
Adj- R^2	0.9578	0.9505	0.9861
$\chi 2$	0.7874	0.3907	0.1247
Redlich-Peterson			
a_{RP}	0.6719	0.6448	0.6202
n_{rp}	0.9875	0.8265	0.9914
K_{Rp}	1.4154	1.4265	1.4829
R^2	0.9836	0.9843	0.9754
Adj- R^2	0.9753	0.9766	0.9631
$\chi 2$	0.1465	0.1125	1.0029

The data obtained from the adsorption isotherm studies at different temperatures were employed to determine the thermodynamic parameters. The Van't Hoff plot and thermodynamic parameters are presented in Fig. 4(d) and Table 6. The estimated values of Gibbs' free energy ($\Delta G°$) were all negative, suggesting the adsorption of Ni(II) ions onto PTLP took place spontaneously. Moreover, the decrease in ΔG^0 with increasing temperature indicates that higher temperatures are more favorable for Ni(II) adsorption. According to the literature, if the value of ΔG^0 lies between -20 and 0 kJ/mol, physisorption is the predominant mechanism in the adsorption process. As listed in Table 6, the values of ΔG^0 suggest that the adsorption of Ni(II) on the adsorbent is interpreted as physical adsorption [Huang et al., 2022]. The positive value of ΔH^0 implies that the adsorption of Ni(II) is an endothermic process. Furthermore, the positive value of (0.06 kJ/molK) signifies the increasing randomness during the adsorption of Ni(II) ions onto PTLP.

Table 6. Thermodynamic parameters for Ni(II) adsorption on PTLP

Pollutant	Temperature (K)	ΔG^0 (kJ/mol)	ΔH^0 (kJ/mol)	ΔS^0 (kJ/molK)
Ni(II)	293	-4.48	13.10	0.06
	303	-5.08		
	313	-5.68		

3.7 Characterization of PTLP

Characterization of adsorbents is a crucial process for evaluating their physical, chemical, and morphological properties and elucidating the adsorption mechanism. Fig. 6 presents the results of SEM-EDX, BET, FTIR, and zeta potential analysis conducted on the adsorbent. The SEM image (Fig. 6(a)) of PTLP before adsorption reveals a rough, irregular surface of the adsorbent, characterized by sporadic pores. However, after adsorption, as depicted in Fig. 6(c), these pore structures were filled almost entirely with Ni(II) ions. The EDX analysis (Fig. 6(b)) of PTLP reveals that the adsorbent consists mainly of carbon, oxygen, and calcium, alongside trace amounts of silicon, sodium, and sulfur. After Ni(II) adsorption, in the EDX analysis shown in Fig. 6(d), the Ni peak appeared. This result suggests that the heavy metal was successfully adsorped onto the PTLP adsorbent. In general, the surface area and pore size distribution are two of the most critical characteristics of an adsorbent that directly influence the heavy metal adsorption capacity. To this end, the BET surface and pore size analysis were carried out. Fig. 6(e) depicts the N_2 adsorption-desorption isotherm curves and pore size distribution curves of PTLP. According to the International Union of Applied Chemistry, the adsorption-

desorption isotherm curves of the adsorbent correspond to Type V with a H4 hysteresis loop. The type V isotherm shape, especially in the low range of P/P^0 (≈0.3), can signify relatively weak interactions between the adsorbent and adsorbate [Thommes et al., 2015]. The specific surface area (S_{BET}), micropore surface area (S_{mic}), and mesopore surface area (S_{mes}) were 2.0325, 0.8727, and 1.1598 m^2/g, respectively. The total pore (V_{tot}), micropore (V_{mic}), and mesopore (V_{mes}) volumes were 0.009, 0.001, and 0.008 m^3/g, respectively. Moreover, the average pore size diameter of the adsorbent was 193.9 Å. This result indicates that the adsorbent used in Ni(II) adsorption was mesoporous in character, which is consistent with that of the SEM image in Fig. 6(a). The FTIR analysis was carried out to identify the surface functional groups of the adsorbent. The principal structural components of lignocellulosic-based biomass are cellulose, hemicellulose, and lignin [Mahyoob et al., 2022]. The FTIR spectra of PTLP before and after adsorption are depicted in Fig. 6(f). The broad peak between 3330 and 3300 cm^{-1} can be attributed to –OH stretching groups assigned to cellulose [Ross et al., 2021]. The symmetric and asymmetric stretching vibrations of $–CH_2$ and $–CH_3$ were located at 2919 and 2850 cm^{-1}, respectively [Li et al., 2024]. The sharp absorption peak at 2117 cm^{-1} corresponds to C=C from alkene or aromatic amine groups [Suriyakala et al., 2022]. Typically, the stretching vibrations of –C=O (carbonyl), –COOH (carboxyl), and –C–O (ether) groups were observed at 1617, 1314, and 1024 cm^{-1}, respectively [Piccirillo et al., 2017].

The C–H bending vibration belonging to the phenyl groups was observed at 779 cm^{-1} [Suriyakala et al., 2022]. The absorption band at 513 cm^{-1} is related to the inorganic network in the structure of PTLP [Rao et al., 2023]. The zeta potential is a leading indicator for evaluating the surface charge, stability, and interaction between the adsorbent and adsorbate. At the optimum pH value studied, the zeta potential of the adsorbent was -7.09 with a zeta deviation of 4.22, which suggests the adsorbent was of good quality but unstable.

Figure 6. SEM images of (a) before adsorption, (c) after adsorption of PTLP; EDS analysis of (b) before adsorption, (d) after adsorption of PTLP; (e) N2 adsorption/desorption isotherm curves and BJH pore size distribution (inset) of PTLP; (f) FTIR spectra

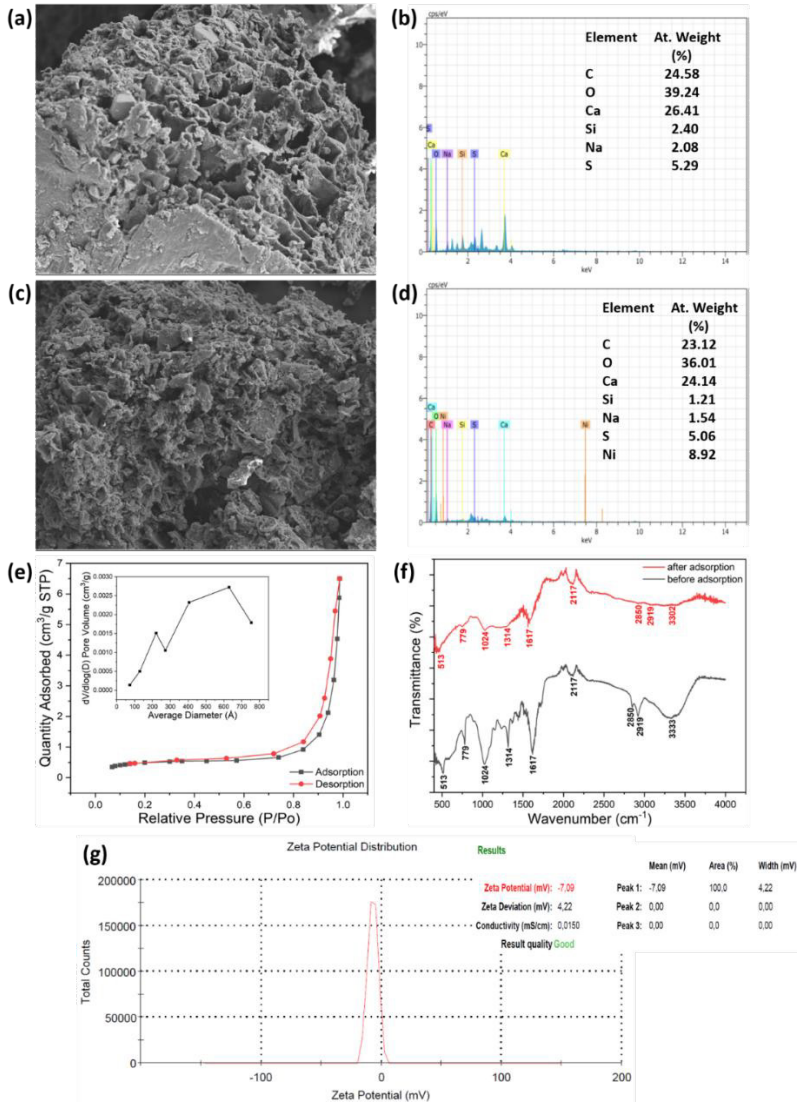

The adsorption of heavy metal ions on a lignocellulosic-based adsorbent can occur through several possible mechanisms, such as pore filling, electrostatic interaction, complexation, precipitation, coordination, chelation, and redox [Meng et al., 2024; Raji et al., 2023]. To expound the adsorption mechanism, the adsorbent before and after the Ni(II) adsorption was analyzed by SEM, FTIR, and zeta potential. Compared to the FTIR images (Fig. 6 (a) and (c)) before and after Ni(II) adsorption, it was observed that the pores on the adsorbent surface were closed entirely. After metal adsorption, no new peak appeared in the FTIR spectrum (Fig. 6(f)). However, the wavenumbers of the oxygen-containing carbonyl and hydroxyl groups shifted from 1617 cm^{-1} and 3333 cm^{-1} to 1610 cm^{-1} and 3302 cm^{-1}, respectively. As depicted in Fig. 6(g), the point of zero charge (pH_{PZC}) of PTLP was -7.09, which implies the surface of the adsorbent was negatively charged. This result suggests the positively charged Ni(II) ions were adsorbed onto PTLP by electrostatic interaction. Moreover, thermodynamic studies confirm that the adsorption process is a physisorption (physical adsorption) process. In summary, Ni (II) adsorption involves pore filling, chelation, electrostatic interactions, and physical adsorption. Fig. 7 illustrates the possible adsorption mechanism of Ni(II) onto PTLP.

Figure 7. Possible adsorption mechanism of Ni(II) onto PTLP

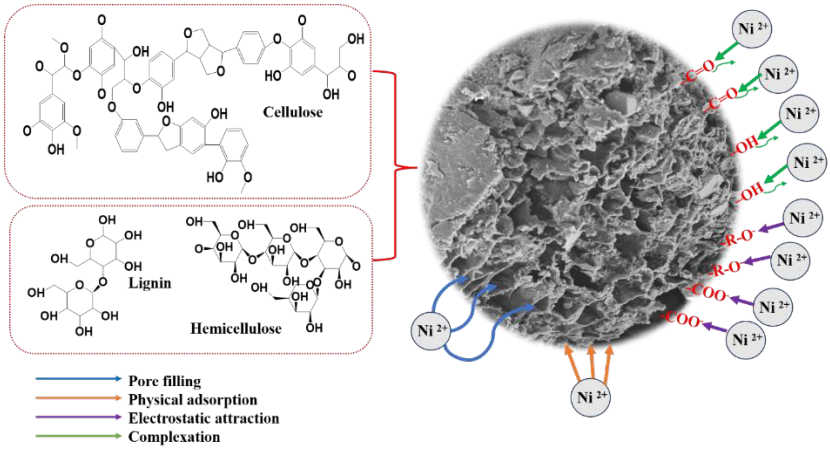

4. CONCLUSIONS

Herein, an adsorbent was prepared facilely from lignocellulosic-based Diospyros Kaki leaves and used to remove Ni(II) ions via adsorption from synthetic wastewater. The experimental results showed that the adsorbent exhibits satisfactory adsorption performance. Adsorption kinetic model studies suggested that the pseudo-second-order kinetic model best fitted the experimental data. Moreover, adsorption isotherm studies revealed that the Langmuir isotherm model could better describe the adsorption character of PTLP with sorption capacities of 18.25, 20.41, and 23.48 mg/g at 20, 30, and 40 °C, respectively. By using spectroscopic and morphological analysis, as well as thermodynamic results, the adsorbent can simultaneously remove Ni(II) ions via multiple mechanisms, including pore filling, physical adsorption, electrostatic interaction, and complexation. This study highlights that tree leaves can be utilized effectively and efficiently as adsorbents, exhibiting good adsorption performance, and can rapidly remove Ni(II) heavy metal ions from wastewater.

ACKNOWLEDGEMENTS

This work was supported by Bilecik Şeyh Edebali University Research Projects Coordination Unit under Grant No. 2017-01.BŞEÜ.03-10. The authors would like to thank the Bilecik Şeyh Edebali University for the financial support.

REFERENCES

Aberdeen, S., Foster, R. I., & Choi, S. (2025). Nickel and cobalt separation via speciation using deep eutectic solvent-based ion exchange. *Separation and Purification Technology, 375*, 133833.https://doi.org/10.1016/j.seppur.2025.133833

Boulanouar, L., Louhichi, B., Hamdi, W., Jellali, S., L'taief, B., Hamdi, N., Rebouh, N. Y., & Houas, A. (2025). Parametric study of cadmium and nickel removal from synthetic and actual industrial wastewater industry by electrocoagulation using solar energy. *Journal of Water Process Engineering, 71*, 107261.https://doi.org/10.1016/j.jwpe.2025.107261

Galera, R. M., da Silva, A. C. P., Jorgetto, A. D. O., Wondracek, M. H. P., Saeki, M. J., Schneider, J. F., Pedrosa, V. d. A., Martines, M. A. U., & Castro, G. R. (2024). Application of the biomass of leaves of *Diospyros kaki* L.f. (Ebenaceae) in the removal of metal ions from aqueous media. *Separations, 11*(1), 12. https://doi.org/10.3390/separations11010012

Gutha, Y., Munagapati, V. S., Naushad, M., & Abburi, K. (2015). Removal of Ni(II) from aqueous solution by *Lycopersicum esculentum* (tomato) leaf powder as a low-cost biosorbent. *Desalination and Water Treatment, 54*, 200–208. https://doi.org/10.1080/19443994.2014.880160

Hadikhani, R., Karbassi, A., Tajziehchi, S., & Mehdizadeh, Y. (2024). Mechanisms and controlling factors of heavy metals removal by electroflocculation in estuarine environments. *Marine Pollution Bulletin, 206*, 116699. https://doi.org/10.1016/j.marpolbul.2024.116699

Huang, Y., Zheng, H., Hu, X., Wu, Y., Tang, X., He, Q., & Peng, S. (2022). Enhanced selective adsorption of lead(II) from complex wastewater by DTPA functionalized chitosan-coated magnetic silica nanoparticles based on anion-synergism. *Journal of Hazardous Materials, 422*, 126856. https://doi.org/10.1016/j.jhazmat.2021.126856

Islam, M. A., Awual, M. R., & Angove, M. J. (2019). A review on nickel(II) adsorption in single and binary component systems and future path. *Journal of Environmental Chemical Engineering, 7*(5), 103305.https://doi.org/10.1016/j.jece.2019.103305

Kashif, M., Akhtar, K., ., & Mustafa, R. (2017). An overview of dermatological and cosmeceutical benefits of *Diospyros kaki* and its phytoconstituents. *Revista Brasileira de Farmacognosia, 27*(5), 650–662. https://doi.org/10.1016/j.bjp.2017.06.004

Khumaidi, A., Murwanti, R., Damayanti, E., & Hertiani, T. (2025). Empirical use, phytochemical, and pharmacological effects in wound healing activities of compounds in Diospyros leaves: A review of traditional medicine for potential new plant-derived drugs. *Journal of Ethnopharmacology, 30*(337), 118966. https://doi.org/10.1016/j.jep.2024.118966

Kumar, P. S., & Kirthika, K. (2009). Equilibrium and kinetic study of adsorption of nickel from aqueous solution onto bael tree leaf powder. *Journal of Engineering Science and Technology, 4*(4), 351–363.

Li, J., Cherkasova, T., Nikolaevich, Y. A., & Yuan, P. (2024). Fabrication of electrospun cellulose/ball-milled bone char membranes for fast, efficient and selective sorption of aquatic U(VI). *Colloids and Surfaces A: Physicochemical and Engineering Aspects, 680*(5). https://doi.org/10.1016/j.colsurfa.2023.132646

Mahyoob, W., Alakayleh, Z., Abu Hajar, H. A., Al-Mawla, L., Altwaiq, A. M., Al-Remawi, M., & Al-Akayleh, F. (2022). A novel co-processed olive tree leaves biomass for lead adsorption from contaminated water. *Journal of Contaminant Hydrology, 248*, 104025. https://doi.org/10.1016/j.jconhyd.2022.104025

Martha, R., Mubarok, M., Darmawan, W., Syafii, W., Dumarcay, S., Charbonnier, C. G., & Gérardin, P. (2020). Biomolecules of interest present in the main industrial wood species used in Indonesia—a review. *Journal of Renewable Materials, 9*(3), 399–449. https://doi.org/10.32604/jrm.2021.014286

Mei, Y., Zhuang, S., & Wang, J. (2025). Adsorption of heavy metals by biochar in aqueous solution: A review. *Science of the Total Environment, 968*, 178898. https://doi.org/10.1016/j.scitotenv.2025.178898

Meng, P., Zhang, T., Su, Y., Peng, D., Zhou, Q., Zeng, H., Yu, H., Lun, L., Zhang, N., Zhang, L., & Zheng, L. (2024). Cellulose-based materials in the treatment of wastewater containing heavy metal pollution: Recent advances in quantitative adsorption mechanisms. *Industrial Crops and Products, 217*(1), 118825. https://doi.org/10.1016/j.indcrop.2024.118825

Murali, P., Shams, R., & Dar, A. H. (2023). Insights on nutritional profile, nutraceutical components, pharmacological potential, and trending utilization of persimmon cultivars: A review. *Food Chemistry Advances, 3*, 100431. https://doi.org/10.1016/j.focha.2023.100431

Piccirillo, C., Moreira, I. S., Novais, R. M., Fernandes, A. J. S., Pullar, R. C., & Castro, P. M. L. (2017). Biphasic apatite-carbon materials derived from pyrolysed fish bones for effective adsorption of persistent pollutants and heavy metals. *Journal of Environmental Chemical Engineering, 5*, 4884–4894. https://doi.org/10.1016/j.jece.2017.09.010

Raji, Z., Karim, A., Karam, A., & Khalloufi, S. (2023). Adsorption of heavy metals: Mechanisms, kinetics, and applications of various adsorbents in wastewater remediation—A review. *Waste, 1*(3), 775–805. https://doi.org/10.3390/waste1030046

Rao, B.N., Rao, P.T., Basha, S.E. *et al.* (2023). Optical response of Eu^{3+}-activated $MgAl_2O_4$ nanophosphors for Red emissive. *Journal of Materials Science: Materials in Electronics,* 34, 955. https://doi.org/10.007/s10854-023-10341-w

Rauf, A., Uddin, G., Patel, S., Khan, A., Halim, S. A., Bawazeer, S., Ahmad, K., Muhammad, N., & Mubarak, M. S. (2017). *Diospyros*, an under-utilized, multi-purpose plant genus: A review. *Biomedicine & Pharmacotherapy, 91*, 714–730. https://doi.org/10.1016/j.biopha.2017.05.012

Ross, M. E., Stanley, M. S., Day, J. G., & Semião, A. J. C. (2021). Removal of metals from aqueous solutions using dried *Cladophora parriaudii* of varying biochemical composition. *Journal of Environmental Management, 290*, 112620. https://doi.org/10.1016/j.jenvman.2021.112620

Saod, W. M., Alaallah, N. J., Abdulkareem, E. A., Hilal, N. N., & AlBiajawi, M. I. (2025). Study of effective removal of nickel and cobalt from aqueous solutions by FeO@mSiO2 nanocomposite. *Results in Chemistry, 13*, 101992. https://doi.org/10.1016/j.rechem.2024.101992

Shahedi, A., Jamshidi-Zanjani, A., Hodadadi Darban, A., Homaee, M., & Taghipour, F. (2025). Nickel, cyanide, zinc, and copper removal from the effluent using photo-electrocoagulation-oxidation. *Journal of Hazardous Materials Advances, 17,* 100550. https://doi.org/10.1016/j.hazadv.2024.100550

Sharma, S., Sharma, M., Kumar, R., Akhtar, M. S., Umar, A., Alkhanjaf, A. M., & Baskoutas, S. (2024). Recent advances and mechanisms of microbial bioremediation of nickel from wastewater. *Environmental Science and Pollution Research International, 31*(28), 40224–40244.https://doi.org/10.10007/s11356-023-30556-y

Soni, H., Kanjariya, P., Ballal, S., Panigrahi, R., Ariffin, I. A., Tantawi, D., Abosaoda, M. K., Nathiya, D., Jayabalan, K., & Chauhan, A. S. (2025). Recent advances in the synthesis of magnetic nanocomposites for the adsorption of heavy metal ions from wastewater. *Journal of Molecular Structure*, 143019. https://doi.org/10.1016/j.molstruc.2025.143019

Suriyakala, G., Sathiyaraj, S., Devanesan, S., AlSalhi, M. S., Rajasekar, A., Maruthamuthu, M. K., & Babujanarthanam, R. (2022). Phytosynthesis of silver nanoparticles from *Jatropha integerrima* Jacq. flower extract and their possible applications as antibacterial and antioxidant agent. *Saudi Journal of Biological Sciences, 29*(2), 680–688. https://doi.org/10.1016/j.sjbs.2021.12.007

Thommes, M., Kaneko, K., Neimark, A. V., Olivier, J. P., Rodriguez-Reinoso, F., et al. (2015). Physisorption of gases, with special reference to the evaluation of surface area and pore size distribution (IUPAC Technical Report). *Pure and Applied Chemistry, 87*(9–10), 1051–1069. https://doi.org/10.1515/pac-2014-1117

Tian, Q., Zhu, Z., Jiang, Y., Zhao, B., Yang, D., Qiu, F., & Zhang, T. (2025). Upcycling of nickel from electroplating sludge as spinel/MnO2 nanowires membrane for durable emulsion separation in harsh environments. *Chemical Engineering Journal, 507*, 160508. https://doi.org/10.1016/j.cej.2025.160508

Tsai, T.-H., Chou, H.-W., & Wu, Y.-F. (2020). Removal of nickel from chemical plating waste solution through precipitation and production of microsized nickel hydroxide particles. *Separation and Purification Technology, 251*, 117315. https://doi.org/10.1016/j.seppur.2020.117315

Vilvanathan, S., & Shanthakumar, S. (2016). Removal of Ni(II) and Co(II) ions from aqueous solution using teak (*Tectona grandis*) leaves powder: Adsorption kinetics, equilibrium and thermodynamics study. *Desalination and Water Treatment, 57*, 3995–4007. https://doi.org/10.1080/19443994.2014.989913

Wang, Z. X., Shen, Q., & Gu, Q. F. (2004). Preparation and characterization of persimmon leaves/cellulose blend fiber and comparison with cellulose fiber. *Carbohydrate Polymers, 57*(4), 415–418. https://doi.org/10.1016/j.carbpol.2004.05.017

Xie, C., Xie, Z., Xu, X., & Yang, D. (2015). Persimmon (*Diospyros kaki* L.) leaves: A review on traditional uses, phytochemistry and pharmacological properties. *Journal of Ethnopharmacology, 163*, 229–240. https://doi.org/10.1016/j.jep.2015.01.007

Yin, H., Wang, B., Zhang, M., & Zhang, F. (2024). Adsorption of Pb(II) in water by modified chitosan-based microspheres and the study of mechanism. *International Journal of Biological Macromolecules, 277*(Pt 1), 134062. https://doi.org/10.1016/j.ijbiomac.2024.134062